CHALMERS
UNIVERSITY OF TECHNOLOGY

# Phase transitions in Bose-Einstein condensates

## A numerical examination of supersolidity in spin-orbit coupled quantum gas

Master's thesis in Physics

Markus Bertilsson & Erik Svensson

DEPARTMENT OF PHYSICS AT THE UNIVERSITY OF GOTHENBURG

CHALMERS UNIVERSITY OF TECHNOLOGY
Gothenburg, Sweden 2022
www.chalmers.se

Master's thesis 2022

# Phase transitions in Bose-Einstein condensates

A numerical examination of supersolidity in spin-orbit coupled quantum gas

Markus Bertilsson and Erik Svensson


CHALMERS
UNIVERSITY OF TECHNOLOGY

Department of Physics at the University of Gothenburg
Chalmers University of Technology
Gothenburg, Sweden 2022

Phase transitions in Bose-Einstein condensates
A numerical examination of supersolidity in spin-orbit coupled quantum gas
Markus Bertilsson and Erik Svensson



Supervisor: Johannes Hofmann , Department of physics at University of Gothenburg
Examiner: Bernhard Mehlig, Department of physics at University of Gothenburg

Master's Thesis 2022
Department of Physics
Chalmers University of Technology
SE-412 96 Gothenburg
Telephone +46 31 772 1000

Typeset in LaTeX
Printed by Chalmers Reproservice
Gothenburg, Sweden 2022

Phase transitions in Bose-Einstein condensates
A numerical examination of supersolidity in spin-orbit coupled quantum gas
Erik Svensson and Markus Bertilsson
Department of Physics
Chalmers University of Technology

# Abstract

The theory of Bose-Einstein condensates developed by Albert Einstein and Satyendra Nath Bose in 1924 paved the way for what is known today as superfluids, a state of matter defined by the property of having zero viscosity, the creation of which was first observed in 1938. This in turn lead to theories about a counter intuitive state of matter, the supersolid, which would able to flow with zero viscosity, while simultaneously attaining a periodic spatially modulated wave function and showing crystalline properties. Recently in 2019, this state was successfully created in labs by several independent research teams, warranting further studies in the field.

In this thesis, we present a spin-1/2, spin-orbit coupled model of a dressed spin Bose-Einstein condensate, and examine its possibility to obtain a supersolid phase, based on $^{87}$Rb Bose-Einstein condensates created in labs using Raman lasers. For the given Hamiltonian, a parameterized ansatz is presented and minimized. The solutions predicts three distinct phases for the ground state, emerging by varying the coupling strength $\Omega$ to the Raman-laser and in order to test the feasibility of this ansatz, a model for numerical calculations of the ground state was developed. To find the most viable method of time propagation, we compare the implementation of the regular Euler propagation with a Fourier split-step method, of which the latter was found to be far superior, both in accuracy and computational speed. Furthermore the excitation spectrum of the ground state solutions are analyzed, which is done by solving the eigenvalue problem from the coupled Bogoliubov equations for small amplitude oscillations and calculating their quasi-momentum.

By constructing a 1D box of finite size, the ground state mean-field of the system could be calculated by implementing a Fourier split-step method with an imaginary time propagation. In our numerical findings, there exists a region close to the phase transition between the striped and separated phase, where higher Fourier components appear for the ground state, thus indicating that the varitaional model can be further expanded upon. Further, these results showed that the phase transition that took place at $\tilde{\Omega} = 1.2$ is now shifted to $\tilde{\Omega} = 1.28$. By studying the Bogoliubov excitations, it was found that these were close to the single particle solutions. However near the transition line where the relaxed mean-field most promenantely differed from the ansatz, it was found that the quadratic behaviour of the excitation spectrum was altered.

Keywords: Quantum gases, Superfluid, Supersolid, Bose-Einstein condensate, Bogoliubov excitation

# Acknowledgements

We would like to thank our supervisor Johannes Hofmann for the valuable input and thought-provoking questions throughout this process, it has been a real joy.

Markus Bertilsson & Erik Svensson, Gothenburg, June 2022

# Contents

# List of Figures

# List of Tables

# 1
# Introduction

## 1.1 Background

The fundamental theory of Bose-Einstein Condensate (BEC) is by no means a new one, and was first introduced in 1925 when Einstein expanded on the ideas that Bose published in 1924, where he introduced the first theory on quantum statistics [1]. The theory describes a quantum gas at temperatures close to absolute zero, in which bosons obtain a macroscopic occupation of the ground state, where the wavefunction for the full system can be well described by a mean-field, making the condensate behaves much like a singular particle. In 1937 the so called super fluid was discovered in liquid $He^4$ and in 1938 Fritz London extended the theory, making the connection between Bose-Einstein condensates and superfluidity [2]. In 1961, the theoretical framework was expanded upon, where a nonuniform theory for interacting BEC was independently created by Gross and Pitaevskii [3, 4]. This further paved the way for a theorised existence of a BEC with a periodic wavefunction, making this a crystalline structure with superfluid properties, the supersolid, which was first suggested as a possible property of solid helium [5, 6]. This counter-intuitive state of matter eluded experimentalists for almost half a century. However, in 2019 these characteristic traits were experimentally produced by several independent research teams using dipolar gases [7, 8, 9]. Thus, with an increasing amount of studies being published on supersolids, both experimental and theoretical, currently makes this a highly relevant and exciting field of study. One main motivation for this thesis is a paper from 2013, where Li et al. proposed a 1D supersolid striped phase based on spin-orbit coupled Bose-Einstei condensates [10].

Based on this background, this work aims to further study the existence of potential supersolids by numerically examining phase transitions between superfluid and supersolid phases. This will be done based on the models of spin-orbit coupled dressed BEC, experimentally created at NIST [11]. This will be done by finding ground state solutions to the Gross-Pitaevskii equations through imaginary-time evolution and comparing these solutions to analytic solutions based on a variationally minimized ansatz proposed by Yun Li et al [12] and examining its excitation spectrum.

The structure of this report is as follows: in chapter 2 the theory on BEC and Gross-Pitaevskii equation (GPE) will be presented along with how the Spin-orbit coupled dressed states are created and determine certain requirements for a achieving a superfluid state. Further, a variational ansatz is defined in order to get a first

approximation of the expected phase transitions. a section discussing Bogoliubov approximation is also included in order to determine excited states.
Chapter 3 defines the methods used to calculate the ground state energy for the system, through relaxation of the BEC mean fields, as well as the methods used to to calculate the excitations.
The numerical discretization and implementation of the system will be presented in chapter 4. In order ensure that model used are feasible, these will be applied to systems with fully analytical solutions, such as the quantum mechanical harmonic oscillator, a Pöschl-Teller potential and lastly a bright soliton, which is a solution to a BEC.

In chapter 5 the results for the found ground state, in comparison to analytical results will be presented together with calculated excitation spectra. The conclusions based on these results will then be stated in chapter 6, together with some proposals for further studies.

## 1.2 Purpose and goal

In order to further understand more complex systems of supersolids, the ansatz by Yun Li needs to be generalised, adding further modes in the supersolid phase in order to reach a lower ground state. If these states do exist, results from computational studies can be used for reference to compare from future experiments, by redetermining the positons of the predicted phase transitions.

## 1.3 Research questions

This thesis will mainly focus on quantum mechanical model simulations in order to help answer the following questions:

1. Is it possible to numerically refine the ground state proposed by Yun Li and find lower ground state energies?
2. Do these numerically refiened ground states have a significantly altered Bogoliubov excitation spectrum?

## 1.4 Delimitations

In this thesis we will only consider 1D system at zero temperature. The computational gains from this is considerable and with 1D superstripes being presented in previous papers [10], such simulated data could possibly be used to compare against raw data from experiments. Furthermore, it was assumed that no external potential was applied to the system, thus the presence of a trapping potential for instance, was omitted.

# 2

# Theory

This section starts with a theoretical description of BECs and then specifically the spin-orbit coupled BECs. This is followed by the introduction of an ansatz to the mean field solutions of the spin-orbit coupled BECs which is the variationally minimized in order to approximate the ground states, resulting in three separate phases depending omn the so called Raman coupling of the system. Lastly, a description to find excited states is presented using Bogoliubov theory. The fundamental theory of BEC is omitted here, to review the subject, we refer to Reference [13].

## 2.1 Gross-Pitaevskii equation

Assuming that the interaction length of a system is small, i.e. that $r_0 \ll d$, where $d = n^{-1/3}$ and $n$ is the average density, one can assume that the Hamiltonian of the system can be approximated as

$$H = \int \left( \frac{\hbar^2}{2m} \nabla \hat{\Psi}^\dagger(\mathbf{r}) \nabla \hat{\Psi}(\mathbf{r}) \right) d\mathbf{r} + \frac{1}{2} \int \hat{\Psi}^\dagger(\mathbf{r}') \, \hat{\Psi}^\dagger(\mathbf{r}) V(\mathbf{r}' - \mathbf{r}) \, \hat{\Psi}(\mathbf{r}') \, \hat{\Psi}(\mathbf{r}) d\mathbf{r}' d\mathbf{r}, \quad (2.1)$$

where only pair interactions are considered, using the two-body potential $V$ [13]. Further assuming that the momenta of the particles are low, more specifically that $pr_0/\hbar \ll 1$, the system will be well characterized by s-wave scatting, where the system becomes fully described by the scattering length $a$. Thus a potential giving rise to the same scattering length would yield the same system, and one can safely replace the real potential in Equation 2.1 with an effective potential $V_{eff}$ on which perturbation theory can be applied. For this potential one can do the approximation of replacing the field operator $\hat{\Psi}(\mathbf{r})$ with the order parameter $\Psi(\mathbf{r})$. Furthermore if one approximates $\nabla\Psi$ to be small in comparison to the interaction length, one can approximate $r'$ with $r$ for the interaction and one obtains the GPE

$$i\hbar \frac{\partial}{\partial t} \Psi(\mathbf{r}, t) = \left( -\frac{\hbar^2 \nabla^2}{2m} + V_{ext}(\mathbf{r}, t) + g|\Psi(\mathbf{r}, t)|^2 \right) \Psi(\mathbf{r}, t) \quad (2.2)$$

where

$$g = \int V_{eff} = \frac{4\pi\hbar^2 a}{m}, \quad (2.3)$$

and the integral of the effective potential can be evaluated using the Born approximation.

## 2.2 Creation of the Spin-orbit coupled dressed states

The Gross-Pitaevskii equation as described in Equation (2.2), does not alone give rise to the striped phase which is associated with supersolids. In order to achieve this, a self Bose-Einstein condensate is here considered with interacting spin states which has previously been done by considering dressed spin states. The specific model that shall here be examined was first done by Spielmans group at NIST where they achieved this by shining detuned Raman lasers on a BEC made up of $^{87}$Rb atoms, as well as applying a static magnetic field and thus this section will follow their derivations as described by [14, 15, 11].
It can be shown that the interaction of an alkali-metal with an external magnetic field can be expressed as

$$A_{\mathrm{hf}}\mathbf{I}\cdot\mathbf{J}+\frac{\mu_B}{\hbar}\mathbf{B}\cdot\left(g_J\mathbf{J}+g_I\mathbf{I}\right), \tag{2.4}$$

where $A_{\mathrm{hf}}$ is the magnetic dipole hyperfine coefficient and $\mu_B$ is the Bohr magneton [14]. Furthermore $\mathbf{I}$ is here the nuclear angular momentum, $\mathbf{J}=\mathbf{L}+\mathbf{S}$ is the angular momentum contribution from the orbital and electronic spin respectively and the $g$-coefficients are the Landé-factors determining the Zeeman-shifts. Assuming that the Zeeman shift is small, one can approximate the Zeeman effect to be linearly proportional to the total angular momentum $\mathbf{F}=\mathbf{I}+\mathbf{J}$, in which case a linear Zeeman effect in response to a magnetic field $\mathbf{B}$ can be expressed as

$$\frac{\mu_B g_f}{\hbar}\mathbf{B}\cdot\mathbf{F} \tag{2.5}$$

where here

$$g_F=g_J\frac{f(f+1)-i(i+1)+j(j+1)}{2f(f+1)} \tag{2.6}$$

is the so called hyperfine Landé factor.
The applied electromagnetic field from the Raman lasers impose a further contribution to the Hamiltonian, where this interaction is given by two contributions, one scalar and one vector light shift, with amplitudes $u_s$ and $u_v$. The vectorized contribution can be shown to couple to the atoms in the same manner as a magnetic field, and thus this contribution will be denoted $\mathbf{B}_{\mathrm{R}}$, and is defined as

$$\mathbf{B}_{\mathrm{R}}=\frac{iu_v\left(\mathbf{E}^*\times\mathbf{E}\right)}{\mu_B\ \mathrm{g}_J} \tag{2.7}$$

and so the full contribution from the optical potential is given by

$$u_s(\mathbf{E}^*\cdot\mathbf{E})+\frac{\mu_B g_f}{\hbar}\mathbf{B}_{\mathrm{R}}\cdot\mathbf{F}. \tag{2.8}$$

This in turn yield the total Hamiltonian as

$$H_E=u_s\left(\mathbf{E}^*\cdot\mathbf{E}\right)+\frac{\mu_B g_F}{\hbar}\left(\mathbf{B}+\mathbf{B}_{\mathrm{R}}\right)\cdot\mathbf{F}+\frac{A_{\mathrm{hf}}}{2}\left(\mathbf{F}^2-\mathbf{J}^2-\mathbf{I}^2\right). \tag{2.9}$$

Here, since a Bose-Einstein condensate is studied, only the lowest energy manifold of $f = 1$ is considered. Within this manifold the $A_{\text{hf}}$-term is constant and thus the corresponding term can be removed by a redefinition of the ground state. Subsequently there is only an angular momentum dependence on $\mathbf{F}$ left, and so the Bose-Einstein condensate can from here on be described as a spin-1 system, spanned by the basis $|m_f = 1\rangle$, $|m_f = 0\rangle$, $|m_f = -1\rangle$, with the corresponding spin-1 operators

$$F_x = \frac{\hbar}{\sqrt{2}} \begin{bmatrix} 0 & 1 & 0 \\ 1 & 0 & 1 \\ 0 & 1 & 0 \end{bmatrix} \quad F_y = \frac{\hbar}{\sqrt{2}} \begin{bmatrix} 0 & -i & 0 \\ i & 0 & -i \\ 0 & i & 0 \end{bmatrix} F_z = \hbar \begin{bmatrix} 1 & 0 & 0 \\ 0 & 0 & 0 \\ 0 & 0 & -1 \end{bmatrix}. \tag{2.10}$$

Lets now take two lasers pointed at the BEC with a detuning of $\delta$, thus yielding the field $\mathbf{E} = \mathbf{E}_- e^{-i\omega t} + \mathbf{E}_+ e^{-i(\omega+\delta)t}$, and as a consequence yielding the effective magnetic field in accordance with Equation (2.9), of

$$\begin{aligned} \mathbf{B}_{\text{R}} = + \frac{iu_v}{\mu_{\text{B}} g_J} \Big[ &\left(\mathbf{E}_-^* \times \mathbf{E}_-\right) + \left(\mathbf{E}_+^* \times \mathbf{E}_+\right) \\ &+ \left(\mathbf{E}_-^* \times \mathbf{E}_+\right) e^{-i\delta t} + \left(\mathbf{E}_+^* \times \mathbf{E}_-\right) e^{i\delta t} \Big]. \end{aligned} \tag{2.11}$$

Spielmans group here instead studied a time-independent system which was obtained by studying the system rotating about the $z$-axis in the spin space, i.e. studying the Hamiltonian

$$H' = S^\dagger H S - i\hbar S^\dagger \frac{\partial S}{\partial t} \tag{2.12}$$

where $S = e^{-i\delta t F_Z/\hbar}$, in order to make the Hamiltonian time-independent [11, 14]. To carry out this calculation, note that the transformations of the angular momentum operators, are

$$\begin{aligned} F_z &\to F_z, \\ F_\pm &\to F_\pm e^{\pm i\delta t}. \end{aligned} \tag{2.13}$$

This is relevant since a rotating wave approximation is here applied, where all contributions with oscillations of order $\delta t$ or higher will be approximated to be zero. For this purpose the $\mathbf{B}_{\text{R}}$ contribution to the Hamiltonian of Equitation (2.9) is rewritten as

$$\begin{aligned} \mathbf{B}_{\text{R}} \cdot \mathbf{F} &= \frac{iu_v}{\mu_{\text{B}} g_J} \Big[ \left(\mathbf{E}_-^* \times \mathbf{E}_-\right) + \left(\mathbf{E}_+^* \times \mathbf{E}_+\right) + \left(\mathbf{E}_-^* \times \mathbf{E}_+\right) (e^{-i\delta t} - e^{i\delta t}) \Big] \cdot \mathbf{F} \\ &= \frac{iu_v}{\mu_{\text{B}} g_J} \Big[ \left(\mathbf{E}_-^* \times \mathbf{E}_-\right) + \left(\mathbf{E}_+^* \times \mathbf{E}_+\right) + \\ &\left(\mathbf{E}_-^* \times \mathbf{E}_+\right) e^{-i\delta t} - \left(\mathbf{E}_+^* \times \mathbf{E}_-\right) e^{i\delta t} \Big] \cdot (\mathbf{e_z} F_z + \mathbf{e}_+ F_+ + \mathbf{e}_- F_-). \end{aligned} \tag{2.14}$$

Now since we shall only consider linearly polaraized light, the first two terms is here set to zero since if all directions of a vector $\mathbf{v}$ have the same phase, it can be written as $\mathbf{u}e^{i\Theta}$ where $\mathbf{u}$ is some real vector and thus $\mathbf{v} \times \mathbf{v} = \mathbf{u}e^{-i\Theta} \times \mathbf{u}e^{i\Theta} = 0$. In the new frame defined by $S$, this contribution is then

$$\frac{iu_v}{\mu_{\mathrm{B}} g_J}\left[\left(\mathbf{E}_-^* \times \mathbf{E}_+\right)\cdot e_+ F_+ + \left(\mathbf{E}_+^* \times \mathbf{E}_-\right)\cdot e_- F_-\right], \tag{2.15}$$

in addition to rotating terms of order $e^{i\delta t}$ or greater, which are here set to zero in accordance to the rotating frame approximation. Now defining $\mathbf{\Omega}\cdot\mathbf{F}$ to be $\mathbf{B_R}\cdot\mathbf{F}$ in the rotating frame together with the contribution $-i\hbar S^\dagger \partial S/\partial t$, $\mathbf{\Omega}$ is then given as

$$\begin{aligned}\mathbf{\Omega} = &-\frac{u_v}{\hbar}\,\mathrm{Im}\left[\left(\mathbf{E}_-^* \times \mathbf{E}_+\right)\cdot(\mathbf{e}_x - i\mathbf{e}_y)\right]\mathbf{e}_x \\ &-\frac{u_v}{\hbar}\,\mathrm{Re}\left[\left(\mathbf{E}_-^* \times \mathbf{E}_+\right)\cdot(\mathbf{e}_x - i\mathbf{e}_y)\right]\mathbf{e}_y + \delta\mathbf{e}_z\end{aligned} \tag{2.16}$$

and the total Hamiltonian contribution from the Raman laser in the rotating frame becomes

$$U(\mathbf{r}) + \mathbf{\Omega}\cdot\mathbf{F} - i\hbar S^\dagger \frac{\partial S}{\partial t} \tag{2.17}$$

where

$$U(\mathbf{r}) = u_s\left(\mathbf{E}_-^*\cdot\mathbf{E}_- + \mathbf{E}_+^*\cdot\mathbf{E}_+\right). \tag{2.18}$$

The Raman lasers used at NIST, were propagating in the spatial $x$-direction towards one-another with orthogonal polarization and so the corresponding fields were defined as

$$\mathbf{E}_- = Ee^{-i(k_R x+\pi/4)}\mathbf{e}_y, \quad \text{and} \quad \mathbf{E}_+ = Ee^{i(k_R x+\pi/4)}\mathbf{e}_z \tag{2.19}$$

and using the Equations of (2.16) and (2.18), one gets

$$\begin{aligned}U(\mathbf{r}) &= u_s\left(\mathbf{E}_-^*\cdot\mathbf{E}_- + \mathbf{E}_+^*\cdot\mathbf{E}_+\right) = 2u_s E^2, \\ \mathbf{\Omega} &= \delta\mathbf{e}_z + \Omega_R\left[\cos(2k_R x)\,\mathbf{e}_x - \sin(2k_R x)\,\mathbf{e}_y\right]\end{aligned} \tag{2.20}$$

where the $U(\mathbf{r}$ is removed by redefining of the potential. Spielmann's group showed that one could shift the minimum energy levels of the different spin states relative to each other by applying a magnetic field [16]. If one applies a magnetic field in the spatial $z$-direction yielding a linear Zeeman shift in accordance with Equation (2.5) one obtains a contribution of $\omega_z^{(1)}F_z$ as well as a quadratic contribution shown to be, $\hbar\omega_z^{(2)}\left|m_f=0\right\rangle\left\langle m_f=0\right|$ [16]. If one then redefines the ground energy by adding a diagonal constant such that the $|m_f=1\rangle$ state has zero energy at zero momentum, one is left with the total Hamiltonian of

$$H = \begin{pmatrix} \hbar^2\frac{k_x^2}{2m} + \xi + \hbar\omega_z^{(2)} & \frac{\Omega}{2}e^{i2k_0x} & 0 \\ \frac{\Omega}{2}e^{-i2k_0x} & \hbar^2\frac{k_x^2}{2m} & \frac{\Omega}{2}e^{i2k_0x} \\ 0 & \frac{\Omega}{2}e^{-i2k_0x} & \hbar^2\frac{k_x^2}{2m} - \xi + \hbar\omega_z^{(2)} \end{pmatrix} \tag{2.21}$$

where $\Omega = 2\Omega_{\mathrm{R}}$. Here $\xi$ is defined as all the $F_z$ dependence i.e. $\xi = \hbar\omega^{(1)} + \hbar\delta$.
By properly tuning the Raman lasers and the static magnetic field, it was shown that one could achieve a region where $\hbar\omega_z^{(2)} - \xi \approx 0$, such that the $|m_f=0\rangle$ and $|m_f=-1\rangle$ states, have energy minima much lower than the $|m_f=1\rangle$ state, and thus creating a so called detuning of this state at low energies, making it such that the Bose-Einstein condensate is primarily made up of the two lower energy states [11]. One then obtains the so called dressed spin states, which is a spin 1/2 model

with a spin up state $|m_F = 0\rangle = |a\rangle$ and a spin up state $|m_F = -1\rangle = |b\rangle$. By defining $\delta = (\hbar\omega_z^{(2)} - \xi)$ and redefining the ground energy by adding $\delta I_2$, the two dimensional Hamiltonian is described by

$$H = \begin{pmatrix} \hbar^2 \frac{k_x^2}{2m} + \frac{h}{2} & \frac{\Omega}{2} e^{i2k_0 x} \\ \frac{\Omega}{2} e^{-i2k_0 x} & \hbar^2 \frac{k_x^2}{2m} - \frac{h}{2} \end{pmatrix}. \tag{2.22}$$

Furthermore, Spielmans group chose to study particles in the spatially rotating frame defined by the unitary transformation $e^{-i\sigma_Z(k_0 x)}$, in which the Hamiltonian

$$h_0^{\mathrm{SO}} = \begin{pmatrix} \hbar^2 \frac{(k_x - k_0)^2}{2m} + \frac{h}{2} & \frac{\Omega}{2} \\ \frac{\Omega}{2} & \hbar^2 \frac{(k_x - k_0)^2}{2m} - \frac{h}{2} \end{pmatrix} = \frac{\hbar^2}{2m} (k_x - k_0\sigma_z)^2 + \frac{\Omega}{2}\sigma_x + \frac{h}{2}\sigma_z \tag{2.23}$$

is independent of position in space, which is the final form of the single particle Hamiltonian that shall here be studied. Note that this rotation introduces a so called light induced synthetic gauge field given by $k_0\sigma_z \mathbf{e_x}$. Furthermore one can note interactions between momentum and spin operators in this Hamiltonian which is the reason these Bose-Einstein condensates are called spin-orbit coupled quantum gases.

Equation (2.23) is the single particle Hamiltonian of the system that was here studied, however to get the full picture however, the Hamiltonian needs to be extended with self interaction of the condensate, here approximated with the Gross-Pitaevskii equation as given by (2.2). Though since the particles here studied have two states, there are different coupling coefficients depending on which states are interacting, given by a matrix $g$ defined as

$$g = \begin{pmatrix} g_{aa} & g_{ab} \\ g_{ab} & g_{bb} \end{pmatrix}, \tag{2.24}$$

$$H = \left[ h_0^{\mathrm{SO}} + \mathbb{I} g \begin{pmatrix} |\psi_a|^2 \\ |\psi_b|^2 \end{pmatrix} \right] \psi_0. \tag{2.25}$$

If one assumes the interaction matrix to be symmetric, i.e. that $g_{aa} = g_{bb}$, the final Hamiltonian can instead be described as

$$H = h_0^{\mathrm{SO}} + \frac{2G_1}{n} \left( \psi_0^\dagger \psi_0 \right) + \frac{2G_2}{n} \left( \psi_0^\dagger \sigma_z \psi_0 \right) \sigma_z, \tag{2.26}$$

where new coefficients $G_1$ and $G_2$ here introduced are defined as

$$G_1 = \frac{N}{V} \frac{(g_{aa} + g_{ab})}{4}, \quad G_2 = \frac{N}{V} \frac{(g_{aa} - g_{ab})}{4}. \tag{2.27}$$

Stationary solutions $\psi_0$ to this modified Gross-Pitaevskii equation are thus the described by

$$\mu\psi_0 = \left[ h_0^{\mathrm{SO}} + \frac{2G_1}{n} \left( \psi_0^\dagger \psi_0 \right) + \frac{2G_2}{n} \left( \psi_0^\dagger \sigma_z \psi_0 \right) \sigma_z \right] \psi_0. \tag{2.28}$$

## 2.3 Superfluidity and supersolidity in Bose Einstein condensates

The superfluid property is defined by the property of having zero viscosity, from this definition different criteria can be derived and here the so called Landau criterion shall be described. This is derived by assuming a fluid, flowing at a constant velocity $\mathbf{v}$, through a stationary capillary. Furthermore assume that the liquid carries a singular excitation of momentum $\mathbf{q}$, making the total energy of the system $E_0 + \hbar\omega(\mathbf{q})$ where $E_0$ denotes the ground energy of the system and $\hbar\omega(\mathbf{q})$ denotes the excitation energy. Making the Galilean transformation to the frame where the liquid is stationary, the energy $E'$ is given by

$$E' = E + \hbar\omega(\mathbf{q}) + \mathbf{q}\cdot\mathbf{v} + \frac{1}{2}Mv^2. \tag{2.29}$$

In this frame it is easy to see that the spontaneous creation of excitations can only occur when the total energy is decreasing, i.e. when $E' < E_0 \implies \hbar\omega(\mathbf{p}) + \mathbf{p}\cdot\mathbf{v} < 0$. Landau´s criterion of superfluidity thus states that

$$v < \min_{\mathbf{q}} \frac{\hbar\omega(\mathbf{q})}{q}. \tag{2.30}$$

By simply assuming that Equation (2.1) holds, one can show that a Galilean transformation of the mean field transforms as

$$\hat{\Psi}'(\mathbf{r},t) = \hat{\Psi}(\mathbf{r}-\mathbf{v}t,t)\exp\left[\frac{i}{\hbar}\left(m\mathbf{v}\cdot\mathbf{r} - \frac{1}{2}mv^2t\right)\right]. \tag{2.31}$$

A solution in equilibrium, i.e. in a stationary ground stat with zero momentum can then be described as $\sqrt{\zeta}e^{-i\mu t/\hbar}$, where $\zeta$ is simply some normalization constant. Transforming the system to a frame of reference where the solution is moving at velocity $\mathbf{v}$ making the order parameter take the form $\psi_0 = \sqrt{\zeta}e^{iS}$, where

$$S(\mathbf{r},t) = \frac{1}{\hbar}\left[m\mathbf{v}\cdot\mathbf{r} - \left(\frac{1}{2}mv^2 + \mu\right)t\right]. \tag{2.32}$$

Thus one concludes that Landau´s criterion in a Bose-Einstein condensate takes the form of

$$\frac{\hbar}{m}|\nabla S| < \min_{\mathbf{q}} \frac{\hbar\omega(\mathbf{q})}{q}. \tag{2.33}$$

Alternatively for more complex systems, the quasi-momentum of the condensate can be defined as the frequency corresponding to the peak of the spatial Fourier transformation of the mean field.

## 2.4 Analytical ground state approximation

In order to calculate the ground state of the system, one needs to minimize the time-independent GPE, given by Equations (2.25) and (2.28). The general analytical

minimizing solution to these equations are hard to find, however it can be done for some given ansatz. Thus for comparison to the numerical solutions, an ansatz based on the analytical solutions of the single particle system is presented and for which the energy of the self interacting system is variationally minimized (2.23). Here we shall follow the calculations as presented by Yun Li et al. [12].
To simplify the analytical expressions the external trapping potential $V_{ext}$ will be omitted and $\delta = 0$. The ground state condensate will thus have the following ansatz for the spinor wave function:

$$\begin{pmatrix} \psi_a \\ \psi_b \end{pmatrix} = \sqrt{\frac{N}{V}} \left[ C_1 \begin{pmatrix} \cos\theta \\ -\sin\theta \end{pmatrix} e^{ik_1 x} + C_2 \begin{pmatrix} \sin\theta \\ -\cos\theta \end{pmatrix} e^{-ik_1 x} \right], \tag{2.34}$$

where N is the total number of particles in the condensate, V is the volume of the box. For this wave function ,the variational parameters are then $C_1$, $C_2$,$k_1$ and $\theta$. Assuming the mean-field approximation, governed by the Hamiltonian given by Equation (2.25)

$$\begin{aligned} E(\psi_a, \psi_b) = \int d^3r \Bigg[ \begin{pmatrix} \psi_a^* & \psi_b^* \end{pmatrix} h_0^{\mathrm{SO}} \begin{pmatrix} \psi_a \\ \psi_b \end{pmatrix} + \frac{g_{aa}}{2} |\psi_a|^4 \\ + \frac{g_{bb}}{2} |\psi_b|^4 + g_{ab} |\psi_a|^2 |\psi_b|^2 \Bigg] \end{aligned} \tag{2.35}$$

Using the ansatz in Equation (2.34), one can analytically approximate the ground state by minimization of this energy. Beginning with minimization with respect to $k_1$ one obtains from the single particle Hamiltonian in (2.23) one obtains that the full $k_1$-dependence is

$$\begin{aligned} &\int d^3r \Psi^* \frac{1}{2m} \left( p_x^2 - 2k_0 \sigma_z p_x \right) \Psi \\ &= \int d^3r \sqrt{\frac{N}{V}} \left[ C_1^* \begin{pmatrix} \cos\theta \\ -\sin\theta \end{pmatrix} e^{-ik_1 x} + C_2^* \begin{pmatrix} \sin\theta \\ -\cos\theta \end{pmatrix} e^{ik_1 x} \right] \cdot \\ &\cdot \frac{\hbar^2}{2m} \left( k_1^2 \Psi - 2k_1 k_0 \sqrt{\frac{N}{V}} \left[ C_1 \begin{pmatrix} \cos\theta \\ \sin\theta \end{pmatrix} e^{ik_1 x} - C_2 \begin{pmatrix} \sin\theta \\ \cos\theta \end{pmatrix} e^{-ik_1 x} \right] \right) \\ &= \int d^3r \frac{\hbar^2 N}{2mV} \left[ k_1^2 n(x) - 2k_1 k_0 \left( |C_1|^2 (\cos^2\theta - \sin^2\theta) - |C_2|^2 (\sin^2\theta - \cos^2\theta) \right) \right]. \end{aligned} \tag{2.36}$$

Integrating and solving for $\partial / \partial_{k_1} E = 0$, one obtains

$$k_1 = k_0 (|C_1|^2 + |C_2|^2)(\cos^2\theta - \sin^2\theta) \implies \cos 2\theta = \frac{k_1}{k_0} \tag{2.37}$$

using the normalization condition $|C_1|^2 + |C_2|^2 = 1$. This fixes a value of $\theta$, which can be used to obtain the expression for the spins per particle as

$$\begin{aligned} \langle \sigma_z \rangle &= |C_1|^2 (\cos^2\theta - \sin^2\theta) + |C_2|^2 (\sin^2\theta - \cos^2\theta) \\ &= \left( |C_1|^2 - |C_2|^2 \right) \cos 2\theta = \frac{k_1}{k_0} \left( |C_1|^2 - |C_2|^2 \right) \end{aligned} \tag{2.38}$$

$$\begin{aligned}\langle\sigma_x\rangle &= -|C_1|^2 2\cos\theta\sin\theta - |C_2|^2 2\cos\theta\sin\theta \\ &= \sin 2\theta = \sqrt{1-\cos^2 2\theta} = -\frac{\sqrt{k_0^2-k_1^2}}{k_0}.\end{aligned} \tag{2.39}$$

The 1D density modulation of a non-homogeneous density can be calculated as

$$\begin{aligned}n(x) = |\psi|^2 &= \left[\begin{pmatrix}\psi_a^* & \psi_b^*\end{pmatrix}\begin{pmatrix}\psi_a \\ \psi_b\end{pmatrix}\right] \\ &= \frac{N}{L}\left[1 + 2C_1^*C_2\cos\theta\sin\theta e^{-i2k_1x} + 2C_1C_2^*\cos\theta\sin\theta e^{i2k_1x}\right] \\ &= \frac{N}{L}\left[1 + 2|C_1C_2|\cos\theta\sin\theta e^{-i(2k_1x+\phi)} + e^{i(2k_1x+\phi)}\right] \\ &= \frac{N}{L}\left[1 + 2|C_1C_2|\frac{\sqrt{k_0^2-k_1^2}}{k_0}\cos(2k_1x+\phi)\right],\end{aligned} \tag{2.40}$$

where in the first step the normalization condition and trigonometric identity have been used and $V = L$ is the size of the system. Note here that given that $k_1 \neq k_0$ or $k_1 \neq 0$, Equation (2.40) describes a periodic modulated density. Subsequently, using the relative phase $\phi$ between $C_1$ and $C_2$ as well as Equation (2.37) with the trigonometric identity $2\cos\theta\sin\theta = \sin 2\theta$, giving the final expression

$$n(x) = \frac{N}{L}\left[1 + 2|C_1C_2|\frac{\sqrt{k_0^2-k_1^2}}{k_0^2}\cos(2k_1x+\phi)\right] \tag{2.41}$$

and the energy per particle as

$$\varepsilon = \hbar^2\frac{k_0^2}{2m} - \frac{\Omega}{2k_0}\sqrt{k_0^2-k_1^2} - F(\beta)\frac{k_1^2}{2k_0^2} + G_1(1+2\beta), \tag{2.42}$$

where $G_1$ and $G_2$ are defined as in Equation (2.27), $\beta = |C_1|^2|C_2|^2$, and where

$$F(\beta) = \left(\hbar^2k_0^2/m - 2G_2\right) + 4\left(G_1 + 2G_2\right)\beta. \tag{2.43}$$

By now minimizing Equation (2.42) with respect to $k_1$ one obtains

$$\frac{\partial\varepsilon}{\partial k_1} = \frac{\Omega k_1}{2k_0\sqrt{k_0^2-k_1^2}} - F(\beta)\frac{k_1}{k_0^2} = 0 \tag{2.44}$$

yielding two solutions

$$k_1 = 0 \quad \text{or} \quad k_1 = k_0\sqrt{1 - \frac{\Omega^2}{4[F(\beta)]^2}}. \tag{2.45}$$

By analyzing that

$$\frac{\partial^2\varepsilon}{\partial k_1^2} = \frac{\Omega k_0}{2(k_0^2-k_1^2)^{3/2}} - \frac{F(\beta)}{k_0^2} \tag{2.46}$$

one sees that for $\Omega/2 > F(\beta)$, the minimum is at $k_1 = 0$ otherwise the minimum is at the second root in Equation (2.45).

Finally minimizing with respect to $\beta$ it is trivial that for the for $k_1 = 0$ the energy per particle in equation (2.42) $\beta = 0$. In the regime where $\Omega/2 < F(\beta)$, where $k_1$ is given by the second root, the energy is obtained by substitution into Equation (2.42) as

$$\varepsilon = -\frac{\Omega^2}{8F(\beta)} + G_1 + G_2(1 - 4\beta). \tag{2.47}$$

To find the minimization with regards to $\beta$, one here note that the second derivative

$$\frac{\partial^2 \varepsilon}{\partial \beta^2} = -\frac{4\Omega^2(G_1 + 2G_2)^2}{F^3} \tag{2.48}$$

is always negative due to $F(\beta) > 0 \; \forall \; \beta$, since $\beta \in [0, 1/4]$ and thus the minimum is at the limiting values of $\beta$, meaning that the minima using the $k_1 \neq 0$ root is either at

$$\varepsilon(\beta = 0) = -\frac{\Omega^2}{8(\hbar^2 k_0^2/m - 2G_2)} + G_1 + G_2 \tag{2.49}$$

or

$$\varepsilon(\beta = 1/4) = -\frac{\Omega^2}{8(\hbar^2 k_0^2/m + G_1)} + G_1. \tag{2.50}$$

Thus from these minimizations, one sees that there are three different cases which shall from here on be labeled as phases I, II and III, which is ordered by the strength of the Raman coupling needed to create the different phases. They are in order defined and characterized as follows.

- Phase I - Striped phase
  This phase will be defined by having $k_1 \neq 0$ and $\beta = 1/4$ and is characterized by a spin symmetry yielding $\langle \sigma_z \rangle = 0$ and being the only phase which is a superposition of the two plane waves propagating in the $\pm x$-direction and hence giving rise to a density modulation. Thus this will be denoted as the striped phase.

- Phase II - Separated phase
  This phase shall here be denoted as the separated phase due to the fact that $\sigma_z \neq 0$. The solution is a plane-wave solution and is thus characterized by a symmetry breaking where either $C_1 = 0$ or $C_2 = 0$.

- Phase III - Zero momentum phase
  The third phase which is a zero-momentum phase where the with $\langle \sigma_z \rangle = 0$, with a simple flat wave-function and density.

The modulation of the density for phase I can be seen in Figure 2.1, for $\tilde{\Omega} = 1$, where the striped property shows the broken translation symmetry. For an explanation of the tilde-notation, see Section 3.1.
At $\delta = 0$ the transition between the phases is completely determined by the Raman coupling $\Omega$ for given couplings, first solving for the transition between phase I and

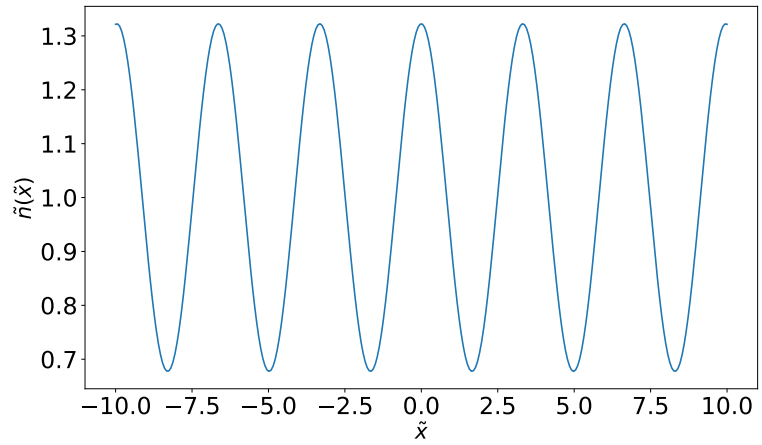


**Figure 2.1:** Density of the ground state for a BEC, where $\tilde{\Omega} = 1$

II. This points is defined by the points at which the energy of phase II becomes greater, i.e. this point would solve

$$\begin{aligned} &\varepsilon(1/4) = \varepsilon(0) \implies \\ &\quad G_2 = -\frac{\Omega^2}{8(\hbar^2 k_0^2/m + G_1)} + \frac{\Omega^2}{8(\hbar^2 k_0^2/m - 2G_2)} \implies \\ &\quad G_2 = \frac{\Omega^2}{8} \frac{G_1 + 2G_2}{(\hbar^2 k_0^2/2m - 2G_2)\,(\hbar^2 k_0^2/m + G_1)} \end{aligned} \tag{2.51}$$

yielding the transition between phases I and II at

$$\Omega^{(\mathrm{I-II})} = 2\left[\left(\hbar^2 k_0^2/m + G_1\right)\left(\hbar^2 k_0^2/m - 2G_2\right)\frac{2G_2}{G_1 + 2G_2}\right]^{1/2} \tag{2.52}$$

Solving instead for $\Omega = 2F(0)$ one obtains the transition between phases II and III at

$$\Omega^{(\mathrm{II-III})} = 2\left(\hbar^2 k_0^2/m - 2G_2\right), \tag{2.53}$$

where in phase III $k_1 = 0$. It is also possible that a transition occurs immediately from phase I to III, which occurs when the criteria $\Omega > 2F(\beta)$ occurs before Equation (2.52) is fulfilled, i.e. when

$$\Omega^{(\mathrm{I-II})} > 2F(\beta) \implies \hbar^2 k_0^2/m > 4G_2 + \frac{4G_2^2}{G_1}. \tag{2.54}$$

This transition then occurs at

$$\varepsilon(k_1 = 0, \beta = 0) = \varepsilon(k_1 = k_0\sqrt{1 - \Omega^2/(4F^2)}, \beta = 1/4) \tag{2.55}$$

or equivalently

$$
\begin{aligned}
&-\frac{\Omega^{(\mathrm{I-III})}}{8(\hbar^2 k_0^2/m+G_1)}+G_1=\frac{\hbar^2 k_0^2/m}{2}-\frac{\Omega^{(\mathrm{I-III})}}{2}+3G_1/2 \implies \\
&\Omega^{(\mathrm{I-III})}=2\left(\hbar^2 k_0^2/m+G_1\right)-2\left[\left(\hbar^2 k_0^2/m+G_1\right)G_1\right]^{1/2}.
\end{aligned} \tag{2.56}
$$

The critical point where the Bose-Einstein condensate start transitioning from phase I to phase III which is defined by the inequality given by Equation (2.54) can be shown to imply a critical value of $G_1$, here denoted $G_1^{(c)}$. This is obtained by solving

$$
\begin{aligned}
\hbar^2\frac{k_0^2}{m}&=4G_2+\frac{4G_2^2}{G_1} \\
&=G_1 4\left(\frac{G_2}{G_1}+\frac{G_2^2}{G_1^2}\right) \\
&=G_1 4\left(\gamma+\gamma^2\right)=G_1 4\gamma\left(1+\gamma\right)
\end{aligned} \tag{2.57}
$$

such that

$$
G_1^{(c)}=\frac{\hbar^2 k_0^2}{4m\gamma\left(1+\gamma\right)}. \tag{2.58}
$$

By using equation (2.27), one can equivalently define a critical density as

$$
\begin{aligned}
n^{(c)}&=\frac{4G_1^{(c)}}{g+g_{ab}}=\hbar^2\frac{k_0^2}{m\left(g+g_{ab}\right)\gamma\left(1+\gamma\right)} \\
&=\hbar^2\frac{k_0^2}{m}\Big/\left(\frac{g^2-g_{ab}^2+\left(g-g_{ab}\right)^2}{g+g_{ab}}\right)=\hbar^2\frac{k_0^2}{m}\Big/\left(2g\frac{g-g_{ab}}{g+g_{ab}}\right) \\
&=\frac{k_0^2}{2g\gamma}.
\end{aligned} \tag{2.59}
$$

This means that the number of possible phase transitions will be dependent on the density of the gas, such that for $n<n^c$ there are two phase transitions, I to II and II to III whereas for $n>n^c$ only a phase transition from I to III is possible.
In Figure 2.2 the main features of the variational ansatz is highlighted. It can be seen that there is a second order phase transition when going from phase 1 to phase 2 by observing the discontinuity of $\tilde{\sigma}_x$ and $\tilde{\sigma}_z$. The phase diagram for the variational ansatz can be seen in Figure 2.3.

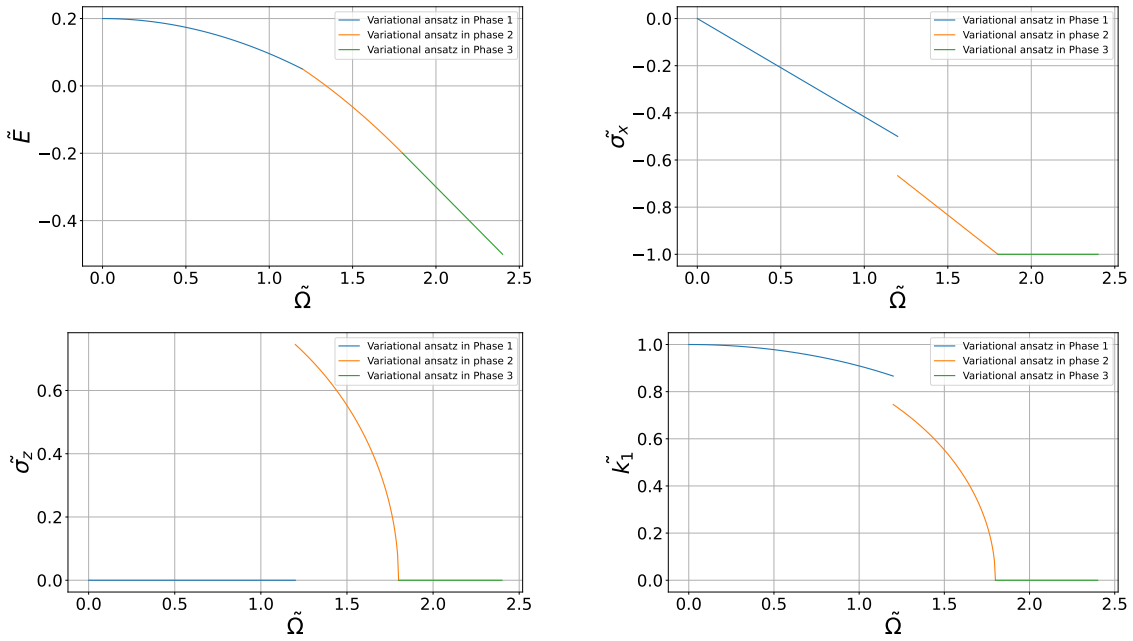


**Figure 2.2:** Plots for the ground state energy $\tilde{E}$, $\tilde{\sigma_x}$, $\tilde{\sigma_z}$ and $\tilde{k_1}$, respectively, for the variational ansatz. In each plot, three distinct phases are shown.

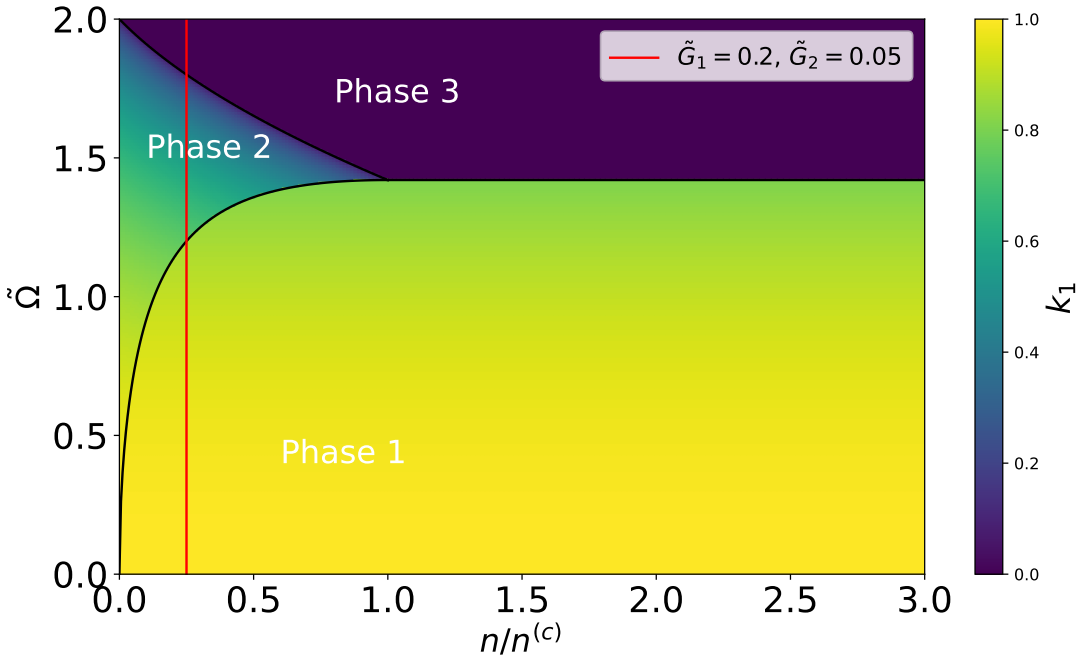


**Figure 2.3:** Phase diagram for the variational ansatz. The red line corresponds to the positions using $G_1 = 0.2$ and $G_2 = 0.05$, which Figure 2.2 is plotted.

## 2.5 Bogoliubov approximation

As was seen in Section 2.3, the excitation spectrum plays an important role in determining the superfluidity and thus supersolidity of the condensate and for this reason the excitation spectrum shall here be examined. This will here be done using Bogoliubov theory, where the time-dependent changes of the mean field is small compared to the stationary solutions. Thus the full field is approximated as

$$\Psi(x,t) = \left[\Psi_0(x) + \Lambda(\mathbf{r},t)\right] e^{-i\mu t/\hbar}, \tag{2.60}$$

where

$$\Lambda = \sum_i \left[u_i(x)e^{-i\omega_i t} + v_i^*(x)e^{+i\omega_i t}\right].$$

One then obtains the relations for $u$ and $v$, by solving the Gross-Pitaevskii equation, i.e. Equation (2.2), using Equation (2.60) as ansatz. After collecting all terms with a frequency dependence of $\pm\omega_i$, one obtains in the spin 0 case,

$$\begin{aligned} \hbar\omega_i u_i &= \left(h_0 - \mu + 2g|\Psi|^2\right) u_i + g\left(\Psi\right)^2 v_i \\ -\hbar\omega_i v_i &= \left(h_0 - \mu + 2g|\Psi|^2\right) v_i + g\left(\Psi_0^*\right)^2 u_i. \end{aligned} \tag{2.61}$$

In the specific case where the mean field $\Psi$ is a real constant, Equation (2.61) can be simplified to

$$\begin{aligned} \hbar\omega u &= \frac{\hbar^2k^2}{2m}u + g\Psi^2(u+v) \\ -\hbar\omega v &= \frac{\hbar^2k^2}{2m}v + g\Psi^2(u+v), \end{aligned} \tag{2.62}$$

which has the solution of

$$(\hbar\omega)^2 = \left(\frac{\hbar^2k^2}{2m}\right)^2 + \frac{\hbar^2k^2}{m}g\Psi^2. \tag{2.63}$$

Note here that for $g = 0$, this simply results in the familiar free particle solution as expected.
If one instead assumes the dressed spin system, and solve for the spin-1/2 Gross-Pitaevskii and thus uses Equation (2.25) one obtains

$$\begin{aligned} \hbar\omega_i \begin{pmatrix} u_{ia} \\ u_{ib} \end{pmatrix} &= \left(h_0^{SO} - \mu\mathbb{I} + \mathbb{I}g\begin{pmatrix} |\Psi_a|^2 \\ |\Psi_b|^2 \end{pmatrix} + g_{ab}\begin{pmatrix} |\Psi_a|^2 & \Psi_b^*\Psi_a \\ \Psi_a^*\Psi_b & |\Psi_b|^2 \end{pmatrix}\right)\begin{pmatrix} u_{ia} \\ u_{ib} \end{pmatrix} + \\ &\qquad \left[\left(\Psi_a, \Psi_b\right) g \begin{pmatrix} \Psi_a \\ \Psi_b \end{pmatrix}\right]\begin{pmatrix} v_{ia} \\ v_{ib} \end{pmatrix} \\ -\hbar\omega_i \begin{pmatrix} v_{ia} \\ v_{ib} \end{pmatrix} &= \left(h_0^{SO} - \mu\mathbb{I} + \mathbb{I}g\begin{pmatrix} |\Psi_a|^2 \\ |\Psi_b|^2 \end{pmatrix} + g_{ab}\begin{pmatrix} |\Psi_a|^2 & \Psi_b\Psi_a^* \\ \Psi_a\Psi_b^* & |\Psi_b|^2 \end{pmatrix}\right)\begin{pmatrix} v_{ia} \\ v_{ib} \end{pmatrix} + \\ &\qquad \left[\left(\Psi_a^*, \Psi_b^*\right) g \begin{pmatrix} \Psi_a^* \\ \Psi_b^* \end{pmatrix}\right]\begin{pmatrix} u_{ia} \\ u_{ib} \end{pmatrix}. \end{aligned} \tag{2.64}$$

Furthermore in the spin-orbit coupled case, for $g = 0$ the excitations become uncoupled from mean field stationary solutions of the Gross-Pitaevskii equation, yielding the eigenvalue equation

$$\omega u = \frac{1}{2}\begin{pmatrix}(q-k_0)^2 & \Omega \\ \Omega & (q+k_0)^2\end{pmatrix} u - \mu u \tag{2.65}$$

for single Fourier mode solutions of momentum $q$. Furthermore $\Omega = 0$ the different spin states of the excitations become uncoupled allowing for simple analytical solutions

$$\begin{aligned}\omega_a &= -\mu + \frac{1}{2}(q-k_0)^2 \\ \omega_b &= -\mu + \frac{1}{2}(q+k_0)^2.\end{aligned} \tag{2.66}$$

Notice here that since the equations for different spin states are uncoupled, one obtains different eigenvalues corresponding to different spin states given by fully separated solutions, for instance

$$\omega_a \begin{pmatrix}u_a \\ 0\end{pmatrix} = \frac{1}{2}\begin{pmatrix}(q-k_0)^2 & 0 \\ 0 & (q+k_0)^2\end{pmatrix} u - \mu \begin{pmatrix}u_a \\ 0\end{pmatrix}. \tag{2.67}$$

For $\Omega \neq 0$, one can instead for $g = 0$ use the ansatz

$$u = \begin{pmatrix}c_1 e^{iqx} \\ c_2 e^{iqx}\end{pmatrix} \tag{2.68}$$

for which one obtains

$$\begin{aligned}\hbar\omega + \mu &= \frac{1}{2}(q-k_0)^2 + \frac{c_2}{c_1}\frac{\Omega}{2} \\ \hbar\omega + \mu &= \frac{1}{2}(q+k_0)^2 + \frac{c_1}{c_2}\frac{\Omega}{2}\end{aligned} \tag{2.69}$$

yielding the solution,

$$\frac{c_2}{c_1} = \frac{2}{\Omega}\left(\hbar\omega + \mu - \frac{1}{2}(q-k_0)^2\right) \tag{2.70}$$

and thus

$$\left(\hbar\omega + \mu - \frac{1}{2}(q+k_0)^2\right)\left(\hbar\omega + \mu - \frac{1}{2}(q-k_0)^2\right) = \frac{\Omega^2}{4} \tag{2.71}$$

where one finally get the relationship

$$\hbar\omega = -\mu + k_0^2 + q^2 \pm \frac{1}{2}\sqrt{4k_0^2q^2 + \Omega^2}. \tag{2.72}$$

# 3
# Methods

In order to find the ground state of our system, we will employ a method consisting of imaginary time evolution. Later, the feasibility of our model is shown with results by comparing our numerical data to analytical solutions. The derivation of these analytical solutions for the simpler system are derived in Appendix A.

## 3.1 Dimensionless quantities

For numerical stability, itwas necessary to use quantities near unity. Thus we shall for all numerical calculations which are based on the dressed spin GPE, i.e. Equations (2.25) and (2.28) use units where

$$\hbar = 1, \quad m = 1, \quad k_0 = 1. \tag{3.1}$$

Thus we shall from here introduce the rescaled quantities denoted, given as for instance

$$\begin{aligned} \tilde{k} &= \frac{k}{k_0} \\ \tilde{E} &= E\frac{m}{\hbar^2 k_0^2} \\ \tilde{x} &= xk_0. \end{aligned} \tag{3.2}$$

Furthermore, other quantities from here on denoted with a tilde will be dimensionless and rescaled in the same manner as the quantities mentioned above. Moreover, one can in Equation (2.35) and (2.28) see that the normalization of the wavefunction, i.e. $\sqrt{N/V}$, can be divided out in all places except for at the quadratic contributions. Thus the dependence on $\sqrt{N/V}$ can be eliminated by a redefinition of $g$ and so we define

$$\tilde{g} = \frac{N}{V}g \tag{3.3}$$

which was used in all simulations and thus the integrated density was set as $\sqrt{N/V} = 1$. This further validates the rescaling of the wavefunction as

$$\tilde{\psi} = \sqrt{\frac{N}{V}}\psi. \tag{3.4}$$

## 3.2 Imaginary Time evolution

To find the ground state of the system, a propagation in imaginary time was preformed, and using the variable change $\tau = -it$, the following equation was solved

$$\frac{\partial}{\partial t}|\psi\rangle = -\frac{i}{\hbar}H|\psi\rangle \implies \frac{\partial}{\partial \tau}|\psi\rangle = -\frac{1}{\hbar}H|\psi\rangle \tag{3.5}$$

with a time evolution expressed as

$$|\psi, t\rangle = e^{-iHt/\hbar}|\psi, 0\rangle \implies |\psi, t\rangle = e^{-H\tau/\hbar}|\psi, 0\rangle. \tag{3.6}$$

This converges to the ground state since

$$|\psi, \tau\rangle = \sum_{n=0}^{+\infty} e^{-H\tau/\hbar}\,|E_n\rangle\,\langle E_n \mid \psi, 0\rangle = \sum_{n=0}^{+\infty} c_n e^{-E_n\tau/\hbar}\,|E_n\rangle\,. \tag{3.7}$$

Thus the ground state will converge to zero slower than every other energy eigenstate and with repeated normalization the full system, a convergence to $|E_0\rangle$ when $\tau \to \infty$ was obtained.

## 3.3 Elementary excitations

Using the stationary ground states found through the imaginary time evolution, the Bogoliubov equations given by Equation (2.61) was then solved. Note that this differential equation is linear in $u_i$ and $v_i$ and thus it was solved by finding the eigenvalues to the matrix corresponding to the equation. The matrix was implemented as a square matrix with size $4N \times 4N$ where $N$ is the number of points use to discretize the spatial dimension, operating on a vector consisting of $\{u_a, u_b, v_a, v_b\}$. Thus the equation solved was

$$\omega \begin{pmatrix} u \\ v \end{pmatrix} = \sigma_z \begin{pmatrix} h_0^{SO} - \mu\mathbb{I} + \Gamma & \left[\left(\Psi_a, \Psi_b\right) g \begin{pmatrix} \Psi_a \\ \Psi_b \end{pmatrix}\right] \\ \left[\left(\Psi_a^*, \Psi_b^*\right) g \begin{pmatrix} \Psi_a^* \\ \Psi_b^* \end{pmatrix}\right] & h_0^{SO} - \mu\mathbb{I} + \Gamma \end{pmatrix} \begin{pmatrix} u \\ v \end{pmatrix}. \tag{3.8}$$

Here $h_0^{SO}$ which is the spin-orbit coupled Hamiltonian defined in Equation (2.23), is a matrix operating on the two component spinor indices as well as the positional. Moreover, $g$ is here the usual coupling matrix operating on the spinor indices and $\Gamma$ is a spinor coupling term introduced in Equation (2.64), defined as

$$\Gamma = g_{ab} \begin{pmatrix} |\Psi_a|^2 & \Psi_b^*\Psi_a \\ \Psi_a^*\Psi_b & |\Psi_b|^2 \end{pmatrix}. \tag{3.9}$$

To then find the excitation spectrum of Bogoliubov excitations, the momentum of the excitation has to be considered. Since the solutions were not assumed to be singular Fourier components, the quasi-momentum $q$ was instead considered which was defined as frequency component corresponding to the peak of the Fourier spectrum. This was done for each excitation component $u_a$, $u_b$, $v_a$ and $v_b$ for each corresponding

eigenvalue and the full excitation spectrum was taken to be all of the quasi-momenta for each excitation component. To reiterate the full method was done as follows:

1. Finding eigenvectors of Equation (3.8).
2. Splitting up the eigenvalue solutions in the four components $u_a$, $u_b$, $v_a$, $v_b$.
3. Calculate the absolute value of the Fourier spectrum for each component
4. Find the frequency corresponding to the the peak of each Fourier spectrum
5. Compare all obtained quasi momenta together to their corresponding eigenvalue

# 4

# Numerics

This section describes the numerical methods employed in this thesis. This will cover the discretization of the system, the time propagation methods used as well as define the boundary conditions. Furthermore, these numerical methods are applied to systems with analytically known solutions in order to validate the methods used.

## 4.1 Discretization

In order to discretize a one dimensional system $f(x)$ it was assigned a finite size of length $\tilde{L}$, where the system was defined on the interval $\left[-\tilde{L}/2, \tilde{L}/2\right]$ for which a given wave function $\Psi(\tilde{x}) \to \Psi_m$, where $m = 0, 1, ...l$ such that $\Psi_m = f(m\Delta\tilde{x})$, $f_0 = f(0)$ and $f_l = f(l\Delta\tilde{x}) = f(L)$ where $\Delta\tilde{x}$ is the step size in the discretized system. The momentum operator $p \to -i\hbar\partial_{\tilde{x}}$ was discretized using a central difference method, where the first order derivative was approximated as

$$\frac{\partial\Psi(m\Delta\tilde{x})}{\partial\tilde{x}} \approx \frac{\Psi_{m+1} - \Psi_{m-1}}{2\Delta\tilde{x}} \tag{4.1}$$

and the second order as

$$\frac{\partial^2\Psi(m\Delta\tilde{x})}{\partial\tilde{x}^2} \approx \frac{\Psi_{m+1} - 2\Psi_m + \Psi_{m-1}}{(\Delta\tilde{x})^2}. \tag{4.2}$$

The discretization for the time was done in a similar fashion as $\Psi(\tilde{x}, t) \to \Psi_m^n$ where $n = 0, 1..., \tau$ such that $\Psi_m^n = \Psi(\tilde{x}, t = n\Delta t)$, $\Psi_m^0 = \Psi(\tilde{x}, t = 0)$ and $\Psi_m^\tau = \Psi(\tilde{x}, T)$ where $T = \tau\Delta t$ is the total time that the system is propagated. The discretization scheme can be seen in Figure 4.1.

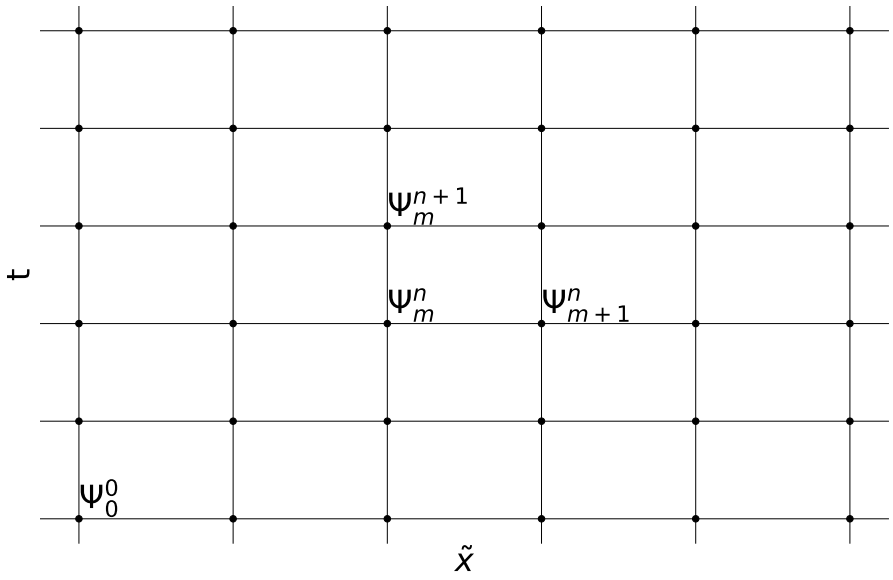


**Figure 4.1:** Schematic figure of the discretization of the wavefunction $\Psi$ in space and time.

## 4.2 Boundary condition and system size optimisation

Due to the fact that periodic solutions were expected as presented in Section 2.4, periodic boundary conditions were used, so that $\Psi_{l+1} = \Psi_0$. An important consequence of this is that the energy of the system becomes dependent on the size of the discretized system. This can for instance be realized by looking at the ansatz solution of Equation (2.34) and seeing that for continuity to hold using periodic boundary conditions, the box size must be equal to the mean-field momentum modulus $2\pi$ times some integer.
For this reason, the $\tilde{L}$ was found which minimizes the ground state solutions with the method discussed in Section 3.2 by calculating the energy according to Equation (2.35). This will be repeated for a set of parameters.

## 4.3 Euler forward

In order to determine the stationary ground state of the system, the system was propagated through time. One simple method of doing this is naturally through the forward Euler method, by numerically propagating the system as

$$\Psi(t + \Delta t) = \Psi(t) - iH(t)\Delta t/\hbar \tag{4.3}$$

which for the imaginary time evolution simply becomes

$$\Psi(\tau + \Delta\tau) = \Psi(\tau) - H(\tau)\Delta\tau/\hbar. \tag{4.4}$$

## 4.4 Split-step Fourier method

A state $|\psi(t)\rangle$ governed by the equation

$$i\hbar\frac{\partial}{\partial t}|\psi(t)\rangle = \hat{H}|\psi(t)\rangle. \tag{4.5}$$

has the time evolution of

$$|\psi, t\rangle = \hat{U}(t)|\psi, 0\rangle, \tag{4.6}$$

where $\hat{U}(t) = e^{-i\hat{H}t/\hbar}$. Thus the total time evolution of a quantum mechanical system can be expressed by repeatedly applying the operator $\hat{U}(\Delta t)$ for a small time step $\Delta t$ such that for propagating a system from $t = 0$ to $t = T$ one has that

$$|\psi, T\rangle = \prod_{n=1}^{N} \hat{U}(n\Delta t)|\psi, 0\rangle. \tag{4.7}$$

By now splitting the Hamiltonian into a kinetic term $\hat{T}$ and other terms $\hat{V}$

$$\exp(-\frac{i}{\hbar}(\hat{T} + \hat{V})\Delta t) = \exp(-\frac{i}{\hbar}\hat{T}\Delta t)\exp(-\frac{i}{\hbar}\hat{V}\Delta t) + O(\Delta t^2), \tag{4.8}$$

where the error in equation 4.8 appears due to the non-commutation between $\hat{T}$ and $\hat{V}$, the time propagation can now be described by implementing the Fast Fourier Transform (FFT):

$$\begin{aligned}
\psi(x, t + \Delta t) &= \left\langle x \left| \exp\left(-\frac{i}{\hbar}\hat{T}\Delta t\right) \exp\left(-\frac{i}{\hbar}\hat{V}\Delta t\right) \right| \psi(t) \right\rangle \\
&= \int dx' \left\langle x \left| \exp\left(-\frac{i}{\hbar}\hat{T}\Delta t\right) \right| x' \right\rangle \exp\left(-\frac{i}{\hbar}V\left(x'\right)\Delta t\right) \psi\left(x', t\right) \\
&= \int dp' \int dx' \left\langle x \mid p' \right\rangle \exp\left(-\frac{i}{\hbar}\frac{p'^2}{2m}\Delta t\right) \left\langle p' \mid x' \right\rangle \exp\left(-\frac{i}{\hbar}V\left(x'\right)\Delta t\right) \psi\left(x', t\right) \\
&= \mathcal{F}^{-1}\left[\exp\left(-\frac{i}{\hbar}\frac{p'^2}{2m}\Delta t\right) \mathcal{F}\left[\exp\left(-\frac{i}{\hbar}V\left(x'\right)\Delta t\right) \psi\left(x', t\right)\right]\right],
\end{aligned} \tag{4.9}$$

as by following a similar procedure in Reference [17]. Using this method, a bigger time step $\Delta t$ can be used in order to reach convergence with fewer iterations in the method explained in the next section.

## 4.5 Validating numerics

To find ground state solutions, the system was evolved through imaginary time by applying the methods presented above. To validate that these methods were implemented correctly we here present them implemented on the harmonic oscillator, Pöschl-Teller potential as well on the Gross-Pitaevskii equation to find the Bright solution solution, the derivation of these can be found Appendix A. The parameters for the following simulations are presented in Table 4.1.

| Propagation method | $P_{\tilde{x}}$ | $\Delta\tilde{x}$ | $\Delta t$ | $P_{\tilde{L}}$ | $\left(\tilde{L}_{min}, \tilde{L}_{max}\right)$ | Iterations |
|---|---|---|---|---|---|---|
| Euler | 600 | $\tilde{L}/P_{\tilde{x}}$ | $0.2\Delta\tilde{x}^2$ | 23 | $(10, 60)$ | $4.5 \cdot 10^5$ |
| Fourier split-step | 600 | $\tilde{L}/P_{\tilde{x}}$ | $0.2\Delta\tilde{x}$ | 23 | $(10, 60)$ | $6 \cdot 10^5$ |

**Table 4.1:** Parameters used for the validation of the method.

### 4.5.1 Harmonic oscillator

In order to test the numerical methods used, they were implemented on a standard harmonic oscillator system. Here the ground state energy was calculated using the imaginary time step method and using two different time-step methods; Euler method and the Fourier split-step method. Using the initial condition of a uniform wave-function,both methods converges close to the true value. However, the convergence is not exact, as can be seen in Figure 4.2. It can also be seen that the Fourier split-step method converged faster and with a smaller error, indicating that it is the preferred method. This is further validated by comparing the ground state wave function to the converged wave function from our numerical method in Figure 4.3.

These difference as small however, as the true ground state energy is $\tilde{E}_{gs} = 0.5$, the energy $\tilde{E}_{sp} = 0.5002$ w obtained, such that the relative error to the ground state remained small.

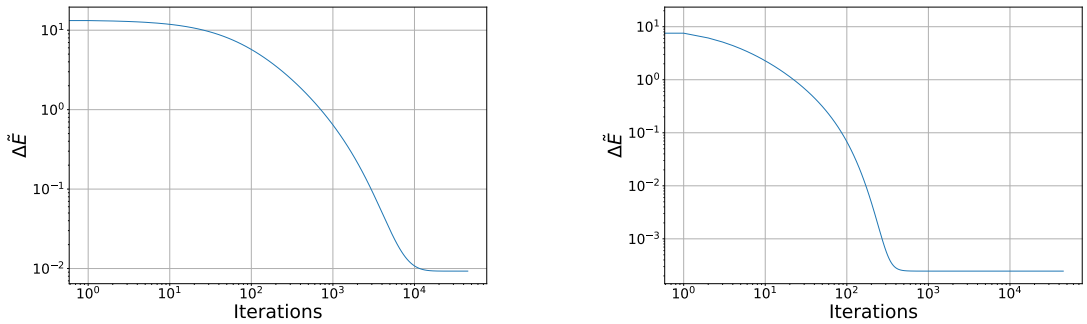


**Figure 4.2:** Figures of the energy convergence $\tilde{E}$ compared to the analytic ground state such that $\Delta\tilde{E} = \tilde{E} - \tilde{E_{gs}}$ for a harmonic oscillator using Euler and split step propagation, respectively, with $\tilde{L} = 60$.

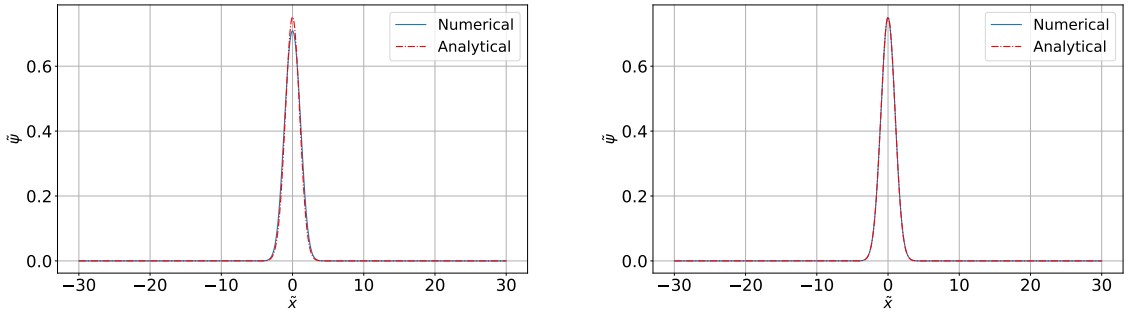


**Figure 4.3:** Figures comparing to the numerically converged wavefunction with analytical ground sate wavefunction using Euler propagation and split-step propagation, respectively.

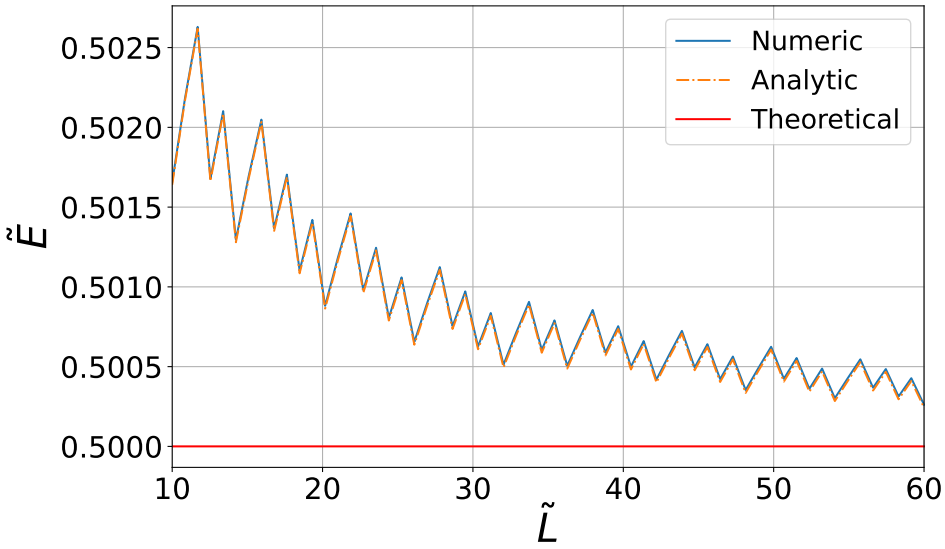


**Figure 4.4:** Figure of ground state energy for a harmonic oscillator using a split step propagation as a function of system size $\tilde{L}$ in blue. The theoretical ground state energy is shown in red, whilst the value when plugging in the analytical wave function into our model is shown in orange.

In figure 4.4 it can be seen that the converged ground state energy using a split step Fourier method is close to the analytical value for the ground state energy for an Harmonic Oscillator. There is also a clear trend that increasing the system size $L$ further will bring the converged numerical value closer to the analytical results. what the periodic "bump" in energy represents is unclear at the moment.

When comparing propagation methods, it can clearly be seen that the split step method is the superior, since convergence is reached faster due to larger time step, but also converging closer to the true ground state energy.

### 4.5.2 Pöschl Teller potential

As for the Harmonic oscillator, the ground state energy diverges for small $L$, but converges to the true ground state energy for a Pöschl-Teller potential, which can be seen to the left in figure 4.5. This is further confirmed by comparing the wave function of the converged ground state with the wave function to he left in Figure 4.5

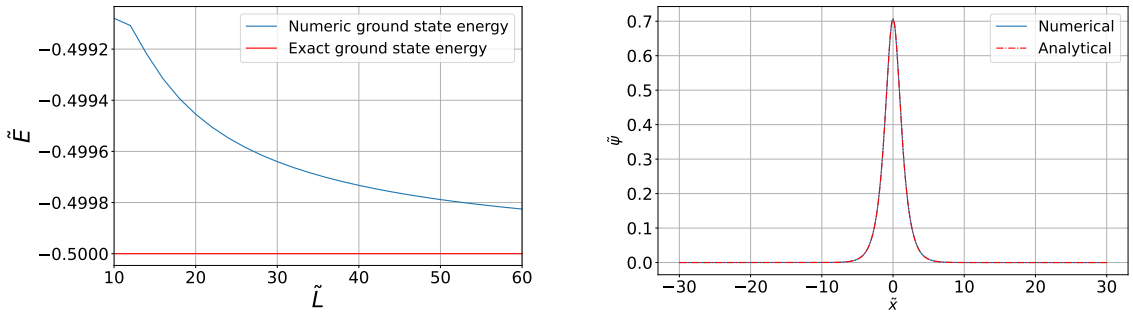


**Figure 4.5:** Figures of the convergence for the ground state energy and comparison of the numerically converged wave function for a Pöschl-Teller potential compared to the analytical ground state wavefunction, respectively, using split-step propagation.

### 4.5.3 Bright soliton

For a one component GPE, the system took longer to converge, so the number of time steps was for the Bright soliton 60000 steps. As for the two previous examples, the calculated ground state energy diverges for small $L$. From Figure 4.6 it can also be seen that a larger is needed for the converged ground state energy to be close to the analytical value. In Figure 4.7 it can be seen that the calculated ground state energy converges to the analytic ground state energy for lower $\tilde{L}$, compared to results for the harmonic oscillator and Pöschl-Teller potential.

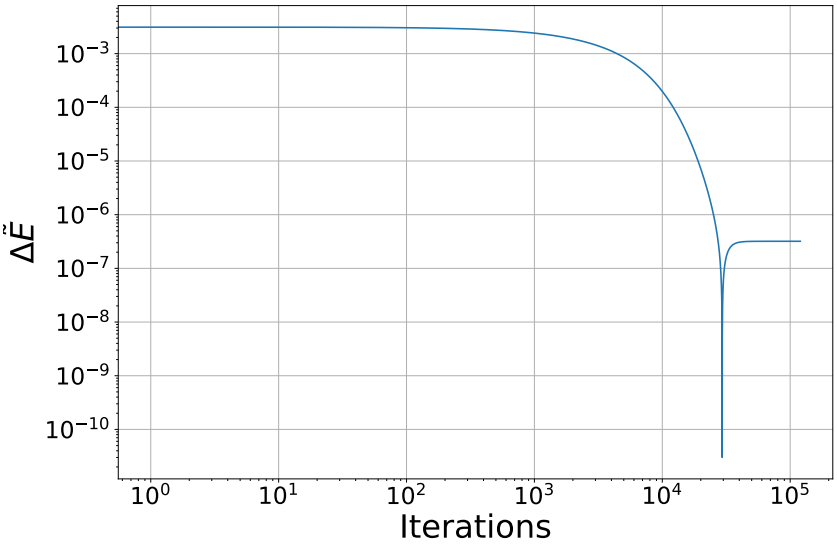


**Figure 4.6:** Plot of the convergence to the ground state of a bright soliton with $\tilde{L} = 60$

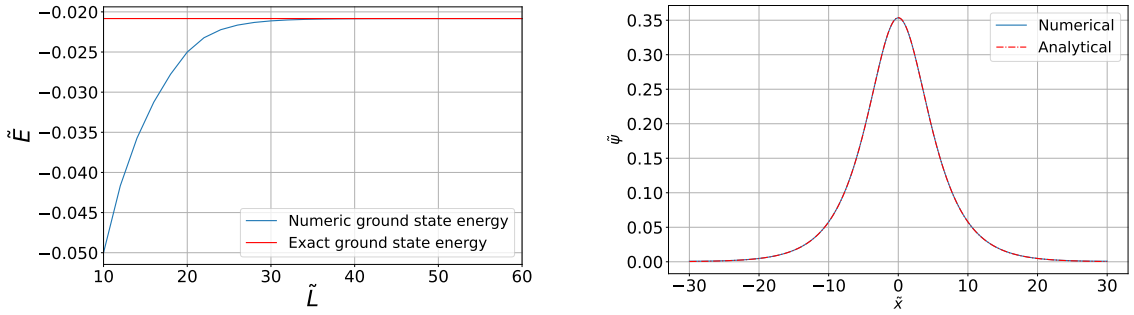


**Figure 4.7:** Figures of the convergence for the ground state energy and comparison of the numerically converged wave function for a bright soliton compared to the analytical ground state wavefunction, respectively, using split-step propagation.

### 4.5.4 Bogoliubov excitations

To examine the validity of the calculations of the Bogoliubov excitations, Equation (2.61) by the methods described above, using a wave function described by a real scalar, with a coupling constant of zero. This was then compared to the analytical solution given by Equation (2.63), yielding the solution

$$\tilde{\omega} = \frac{\tilde{q}^2}{2} \tag{4.10}$$

and in Figure 4.8, this relation is illustrated together with the numerical solutions.

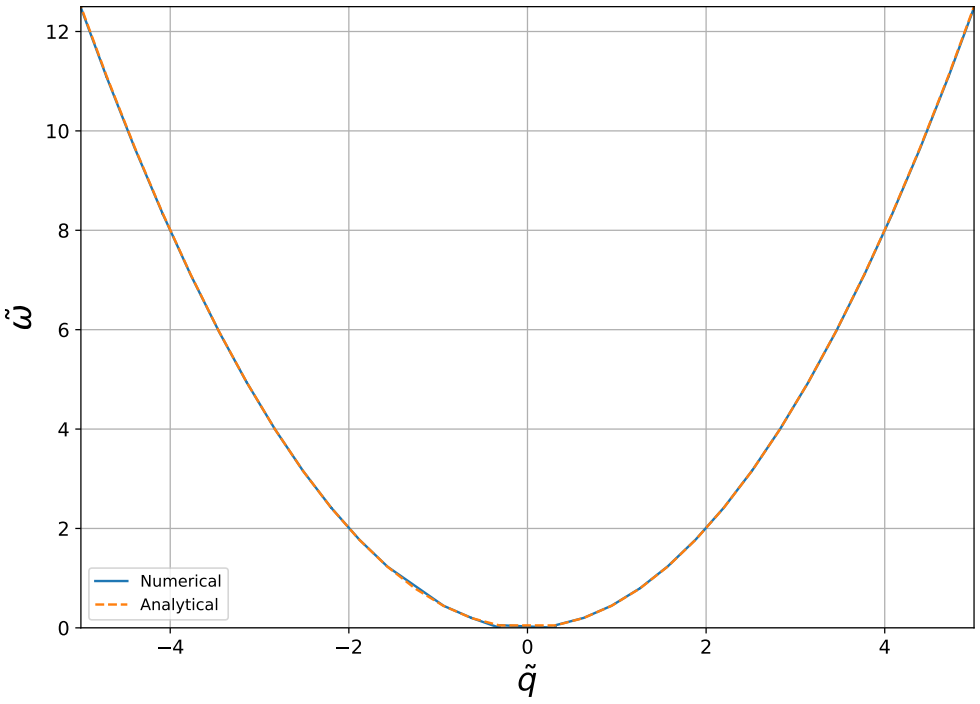


**Figure 4.8**

### 4.5.5 Findings

From these first methods, it is immediate that the benefits of using a split step propagation are two-fold, convergence is reached more rapidly, and the converged values are closer to analytical results. Henceforth, all results will use the Fourier split step method, due to its efficiency and accuracy. Also to note is that since the numerical solution that best approximated the analytical solution was the bright soliton. Since the bright soliton arises from a GPE, it further strengthens the legitimacy of using our method when studying BEC.

# 5
# Results

In this section numerical simulation mean-field energy minimization using the imaginary time evolution was performed, which was done using the analytical ansatz as initial mean-field wave function. The excitation of these were then analyzed using Bogoliubov theory.

## 5.1 Ground state of a Bose-Einstein condensate

For the results in this section, the parameters in Table 5.1 were used for all calculations. Firstly, the ground state energy $\tilde{E}$ is calculated by varying the parameter $\tilde{\Omega}$ and compared to the variational ansatz. Then a region of interest for the $\tilde{\Omega}$-parameter is studied more closely.

| $P_{\tilde{x}}$ | $\Delta\tilde{x}$ | $\Delta t$ | $\tilde{G}_1$ | $\tilde{G}_2$ |
|---|---|---|---|---|
| 1000 | $\tilde{L}/P_{\tilde{x}}$ | $0.2\Delta\tilde{x}$ | 0.2 | 0.05 |

**Table 5.1:** The parameter specifics constant for all simulations

### 5.1.1 Complete sweep

| Run | $P_{\tilde{L}}$ | $(\tilde{L}_{min}, \tilde{L}_{max})$ | $P_{\tilde{\Omega}}$ | $(\tilde{\Omega}_{min}, \tilde{\Omega}_{max})$ | Iterations |
|---|---|---|---|---|---|
| 1 | 60 | $(6, 18)$ | 23 | $(0, 2.3)$ | 10000 |

**Table 5.2:** Table of parameters used for a full sweep of $\tilde{\Omega}$

Using split-step propagation and imaginary time method, the energy dependence of the ground state with respect to the box size $\tilde{L}$ for different Raman couplings $\tilde{\Omega}$ was found for the parameters presented in Table 5.2. For each of the Raman couplings, a sweep over different box sizes $\tilde{L}$ was done for which the energy was calculated. $\tilde{L}$-sweeps for a singular Raman coupling can be seen in Figure 5.1, for $\tilde{\Omega} = 0$ and $\tilde{\Omega} = 2.3$, respectively, for a propagated system using the analytical ansatz as initial mean-field wavefunction. In all propagated systems a total of $P_{\tilde{x}} = 10^3$ spatial points were used, with a time step of $\Delta t = 0.2\Delta\tilde{x}$ and coupling constants $\tilde{G}_1 = 0.2$ and $\tilde{G}_2 = 0.05$. For the simulations shown in Figures 5.1-5.7 a total of

$P_{\tilde{L}} = 60$ different system sizes were used of the space from $\tilde{L} = 6$ to $\tilde{L} = 18$. For the sweep over $\tilde{\Omega}$ a total of 23 points over the space $\tilde{\Omega} = 0$ to $\tilde{\Omega} = 2.3$ were used, and the system was deemed to be converged after a total of $10^4$ iterations.

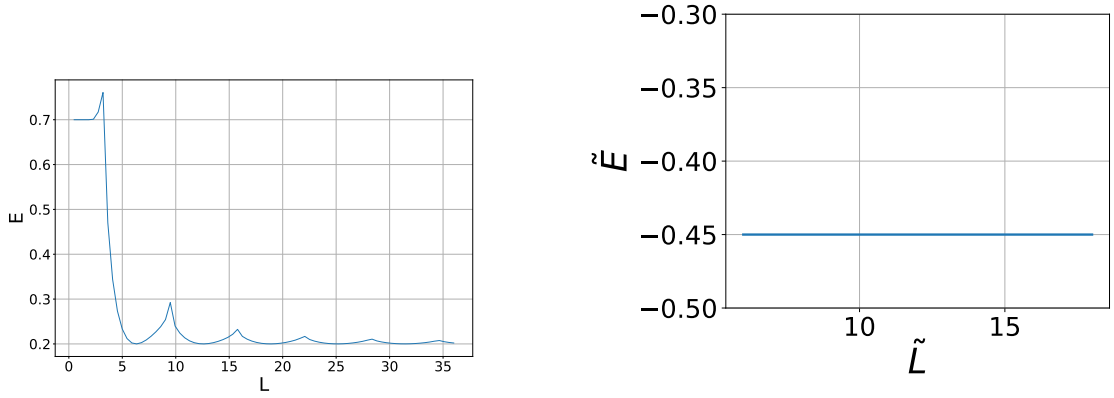


**Figure 5.1:** Ground state energy as a function of the system size for $\tilde{\Omega} = 0$ in the striped phase and $\tilde{\Omega} = 2.3$ in the zero momentum phase, using the analytical ansatz as initial mean-field wavefunction.

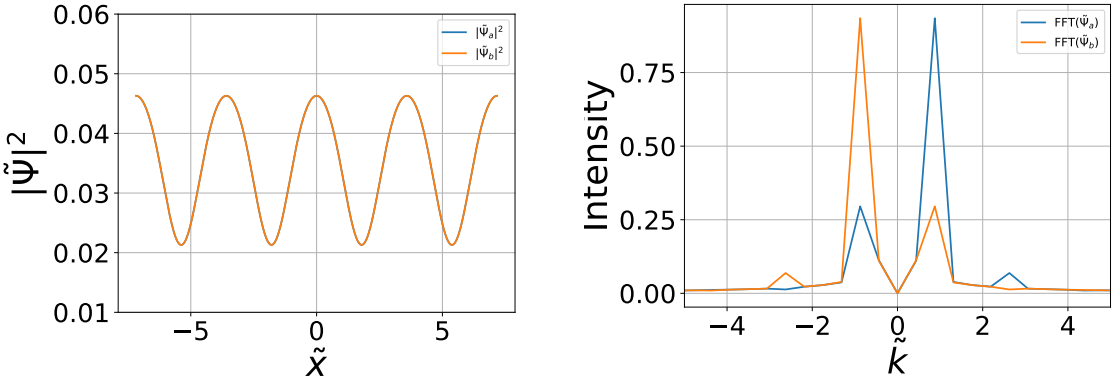


**Figure 5.2:** The full density after propagation, using the optimized box length for $\tilde{\Omega} = 1.05$. Peaks in $\tilde{k}$-spectrum are found at $\pm 0.88$ and $\pm 2.63$.

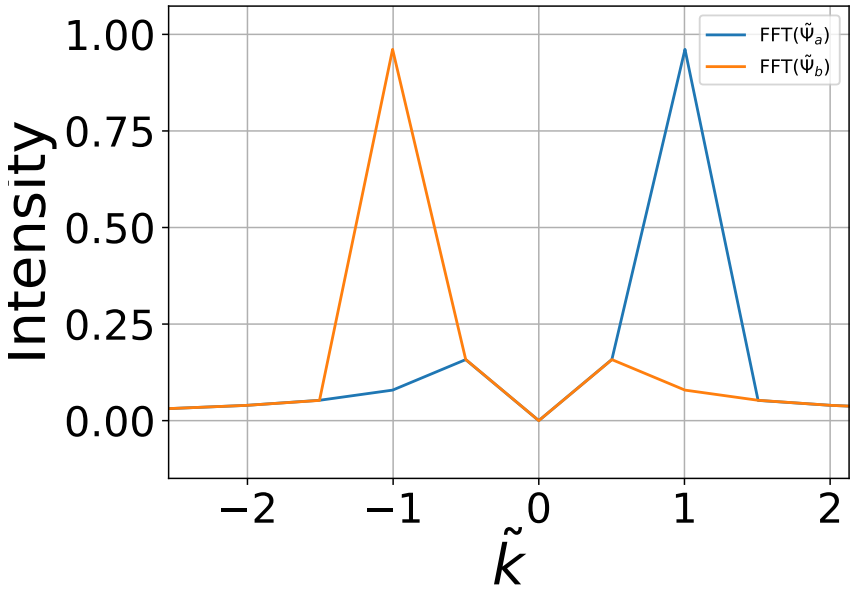


**Figure 5.3:** The Fourier spectrum of the mean field wave functions for $\tilde{\Omega} = 0$.

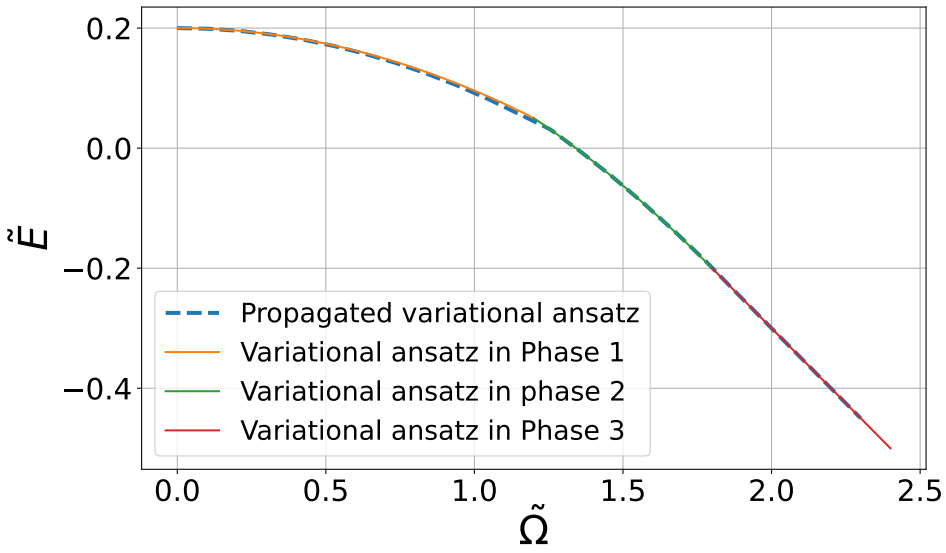


**Figure 5.4:** Ground state energy as a function of the Raman coupling together with analytical results. Here, for the variational yellow is phase I, green II and red phase III.

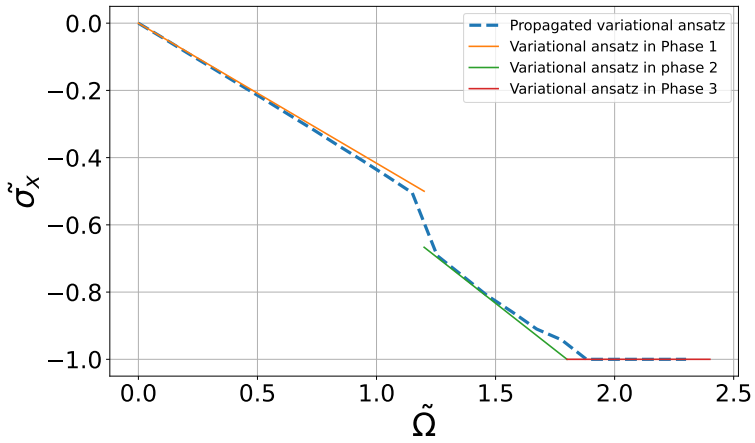


**Figure 5.5:** Transverse spin as a function of the Raman coupling together with analytical results. Here Yellow is phase I, green II and red phase III.

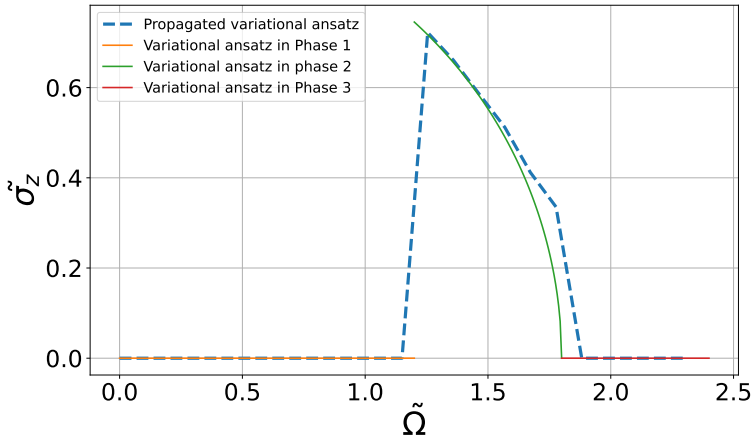


**Figure 5.6:** Spin as a function of the box size together with analytical results. Here Yellow is phase I, green II and red phase III.

As can be seen in Figure 5.1 the ground state energy in our simulations has a periodic behaviour as a function of the box size in the striped phase. We believe that this is due to the fact that the optimal mean-field solution has a periodicity equal to the periodicity of the energy oscillation when changing the box size. Thus when the box size becomes slightly greater than this, the number of oscillations is forced to increase by one and the $\tilde{k_1}$-value of the mean-field becomes offset from the minimizing value. This is implied by the fact that the periodicity of the solution presented in Figure 5.1 is close to $2\pi$. Notice here that this is precisely when a single Fourier mode of momentum $\tilde{k_1} = 1$, which the value predicted from Equation (2.45) for $\tilde{\Omega} = 0$, would be able to fit in a box with periodic boundary conditions without discontinuity. Thus, for the striped face we always expect that $n\tilde{k}_1 2\pi = \tilde{L}$ always holds for the ground state, for any integer $n$. In contrast, for $\tilde{\Omega} = 2.3$, no

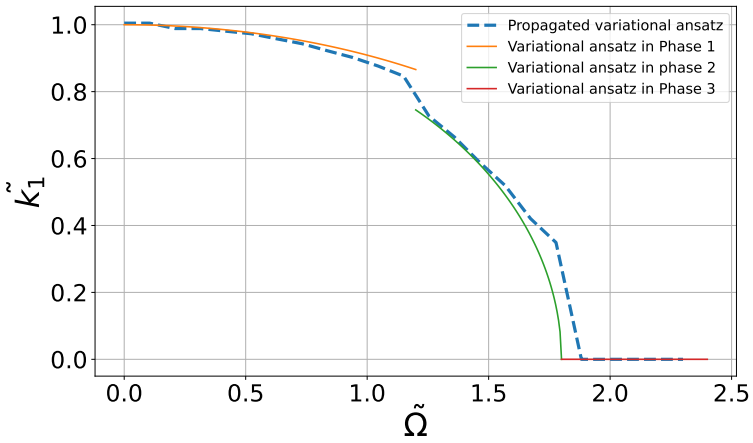


**Figure 5.7:** The dominant wave vector of the Fourier spectrum of the mean-field, together with the solution predicted by that ansatz.

dependence on the box size is found for the energy. This is to be expected, since $\tilde{k}_1$ is always zero, such that the periodic boundary conditions are always met.
As expected, a spatial symmetry breaking for the density in to striped phase was found, which can be seen in Figure 5.2 for $\tilde{\Omega} = 1.05$. This is as predicted by the analytical ansatz, close to being a superposition of two single Fourier modes, which is further implied by the Fourier spectra seen in Figure 5.2, which clearly displays to peaks at $\tilde{k} = \pm 0.88$ for $\tilde{\Omega} = 1.05$, which can be compared to the predicted value of $\tilde{k}_1 = 0.90$. The plot however also displays higher Fourier modes at $\tilde{k} = \pm 2.63$ indicating that the optimal solution is slightly different from the analytical ansatz.
Examining the minimization done over different Raman couplings, the system was shown to closely follow the predictions of the analytical ansatz, in Energy, spin, transverse spin and momentum respectively which is shown in Figures 5.4-5.7. The most noticeable difference can be seen to happen at the second order phase transition, between the striped phase and the separated phase. Looking at Figure 5.4 one sees that the minimized energy of the propagated system is slightly lower, indicating a phase transition at a higher $\tilde{\Omega}$ then predicted. For lower $\tilde{\Omega}$, no such higher Fourier mod is found, as can be seen for $\tilde{\Omega} = 0$ in figure 5.3

### 5.1.2 Raman coupling region of interest

From the results in section 5.1.1, we see a region of $\tilde{\Omega}$-space where the ground state energy is lower compared to the variational ansatz. This suggests that the phase transition from the striped phase to the separated discussed in section 2.4. In order to get more accurate results for this phase transition, the ansatz wave function from both the striped I and the separated (I) phases are studied on the interval for the coupling strength $\tilde{\Omega}$ stated in Table 5.3.
For the simulations presented in Figures 5.8-5.9 a noticeable shift is found in the point for the phase transition, is detected. From the variational ansatz the phase transition is expected at $\tilde{\Omega} = 1.2$, in Figure 5.8 this is now to be found at $\tilde{\Omega} = 1.29$.

| Run | $P_{\tilde{L}}$ | $(\tilde{L}_{min}, \tilde{L}_{max})$ | $P_{\tilde{\Omega}}$ | $(\tilde{\Omega}_{min}, \tilde{\Omega}_{max})$ | Iterations |
|---|---|---|---|---|---|
| 2 | 120 | (20,30) | 23 | (1.1,1.4) | 5000 |

**Table 5.3:** Table of parameters used for the $\tilde{\Omega}$-region of interest.

This is due to the higher Fourier component of the $\tilde{k}_1$-spectrum that can be seen in Figure 5.9.

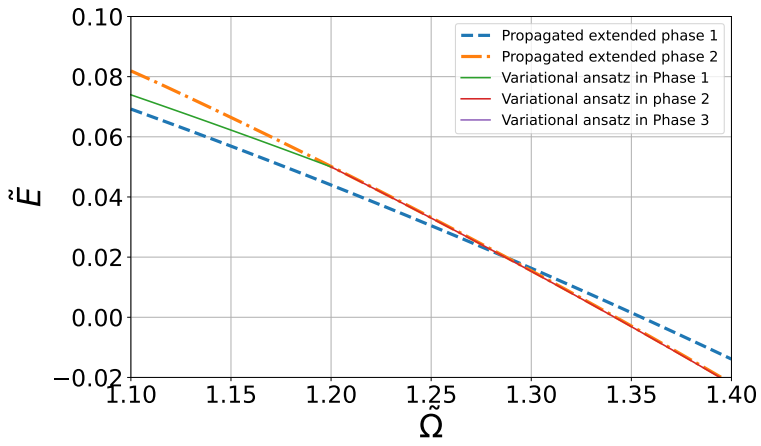


**Figure 5.8:** Plot focusing on the ground state energy in the range $\Omega \in [1.1, 1.4]$. By increasing accuracy and overlapping the wavefunctions for the ansatz in the striped and separated phases, it can be seen that we have a phase transition first closer to $\tilde{\Omega} \approx 1.29$.

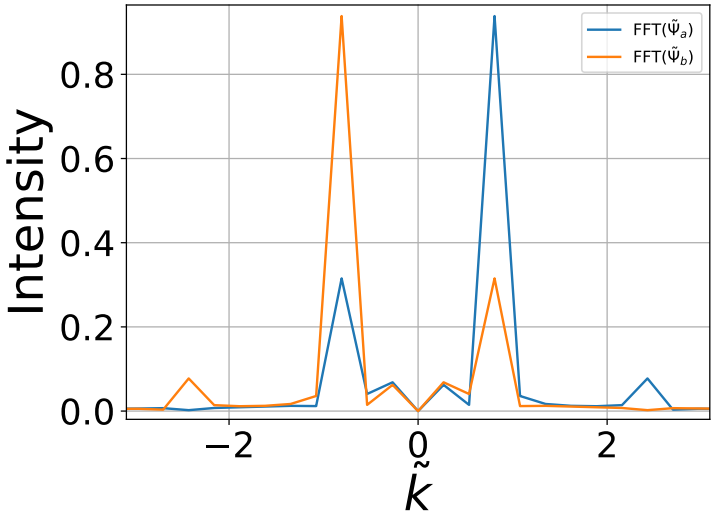


**Figure 5.9:** Fourier spectrum for $\tilde{\Omega} = 1.26$. Here there are higher Fourier component detected, where the low frequency peak is at 0.82, and the high is at 2.44.

## 5.2 Bogoliubov excitations

For the following calculations, further mean-field solutions to the Gross-Pitaevskii equation were found in the same manner as above using the same coupling constants $\tilde{G}_1 = 0.2$ and $\tilde{G}_2 = 0.05$. Here since the resolution of the Fourier spectra scales linearly with the size of the system, these simulations were done using the system size area $\tilde{L} = 90$ to $\tilde{L} = 106$, and to not decrease the spatial point density as greatly the number of spatial points were increased to $2 \cdot 10^3$ points, where the full specifics of the propagation can be seen in Table 5.4.

| $P_{\tilde{L}}$ | $(\tilde{L}_{min}, \tilde{L}_{max})$ | $\tilde{G}_1$ | $\tilde{G}_2$ | $P_x$ | Iterations |
|---|---|---|---|---|---|
| 80 | $(90, 106)$ | 0.2 | 0.05 | 2000 | 5000 |

**Table 5.4:** Run specific parameters in our simulations.

For these mean field solutions, the Bogoliubov excitation spectrum was calculated based on the numerical methods found in Section 3.3. An example of this can be seen in Figure 5.10 where a Raman coupling of $\tilde{\Omega} = 0$ was used. Together with the found solutions, the analytical solutions to the uncoupled system for $g = 0$ and $\tilde{\Omega} = 0$ derived in Section 2.5 are plotted, i.e. the solutions

$$\begin{aligned} \omega_a &= -\mu + \frac{1}{2}(q - k_0)^2 \\ \omega_b &= -\mu + \frac{1}{2}(q + k_0)^2. \end{aligned} \tag{5.1}$$

Notice in Figure 5.10 that the spectrum is approximately mirrored around the $\tilde{q} = 0$. The reason for this can be discerned by studying the Bogoliubov equations (2.64)

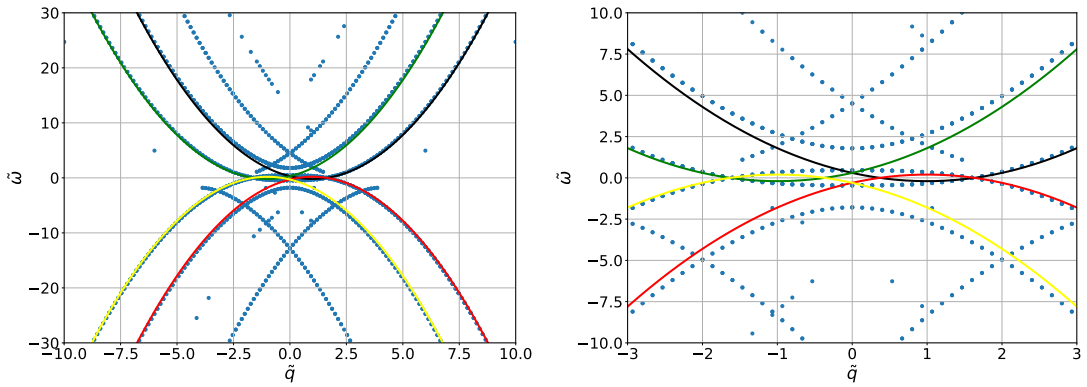


**Figure 5.10:** Excitation spectrum corresponding to the mean field solution minimized using the variational ansatz as initial condition, with parameters $\tilde{\Omega} = 0$, $\tilde{G}_1 = 0.2$, $\tilde{G}_2 = 0.05$. This is plotted together with the single particle relations $\pm\omega = -\mu + \frac{1}{2}(q - k_0)^2$ and $\pm\omega = -\mu + \frac{1}{2}(q + k_0)^2$. The two figures display the same excitation spectrum but for different axis.

and doing the variable change $\omega \to -\omega$ together with the variable change $u \to v$ and $v \to u$. One then finds the very similar system of equations

$$\begin{aligned}
\omega_i \begin{pmatrix} u_{ia} \\ u_{ib} \end{pmatrix} &= \left( h_0^{SO} - \mu\mathbb{I} + \mathbb{I}g \begin{pmatrix} |\Psi_a|^2 \\ |\Psi_b|^2 \end{pmatrix} + g_{ab} \begin{pmatrix} |\Psi_a|^2 & \Psi_b\Psi_a^* \\ \Psi_a\Psi_b^* & |\Psi_b|^2 \end{pmatrix} \right) \begin{pmatrix} u_{ia} \\ u_{ib} \end{pmatrix} + \\
&\qquad \left[ \left( \Psi_{ia}^*, \Psi_{ib}^* \right) g \begin{pmatrix} \Psi_{ia}^* \\ \Psi_{ib}^* \end{pmatrix} \right] \begin{pmatrix} v_{ia} \\ v_{ib} \end{pmatrix} \\
-\omega_i \begin{pmatrix} v_{ia} \\ v_{ib} \end{pmatrix} &= \left( h_0^{SO} - \mu\mathbb{I} + \mathbb{I}g \begin{pmatrix} |\Psi_a|^2 \\ |\Psi_b|^2 \end{pmatrix} + g_{ab} \begin{pmatrix} |\Psi_a|^2 & \Psi_b^*\Psi_a \\ \Psi_a^*\Psi_b & |\Psi_b|^2 \end{pmatrix} \right) \begin{pmatrix} v_{ia} \\ v_{ib} \end{pmatrix} + \\
&\qquad \left[ \left( \Psi_a, \Psi_b \right) g \begin{pmatrix} \Psi_a \\ \Psi_b \end{pmatrix} \right] \begin{pmatrix} u_{ia} \\ u_{ib} \end{pmatrix}.
\end{aligned} \tag{5.2}$$

One here notices that with one last variable change $\Psi \to \Psi^*$ the original coupled equations given by Equation (2.64) are obtained. Furthermore assuming that the solutions are given by the ansatz given by Equation (2.34), which is a close estimation according to the results given above, one realizes that the variable change $\Psi \to \Psi^*$ is equivalent to the variable change $C_1 \to C_2$ and $C_2 \to C_1$. Therefore, the closely mirroring excitation bands are here believed to be solutions to the similar stationary solutions of the conjugate of the mean field. For this reason the mirrored versions of Equation (2.66) are also plotted in the excitation spectrum.
In Figures 5.11 and 5.12, the excitation spectra of the analytical ansatz can be seen together with the propagated solution. This is plotted at the Raman coupling $\Omega = 1.15$, which is just before the analytical prediction of the phase transition, see Figure 5.8, where the deviations from the ansatz are greater. It can here be seen in Figure 5.11 that the quadratic behaviour is somewhat altered and for greater momenta $\tilde{q}$, there is significant alterations of the spectra. However as can be seen in Figure **??** the overlap for small momenta is much greater.

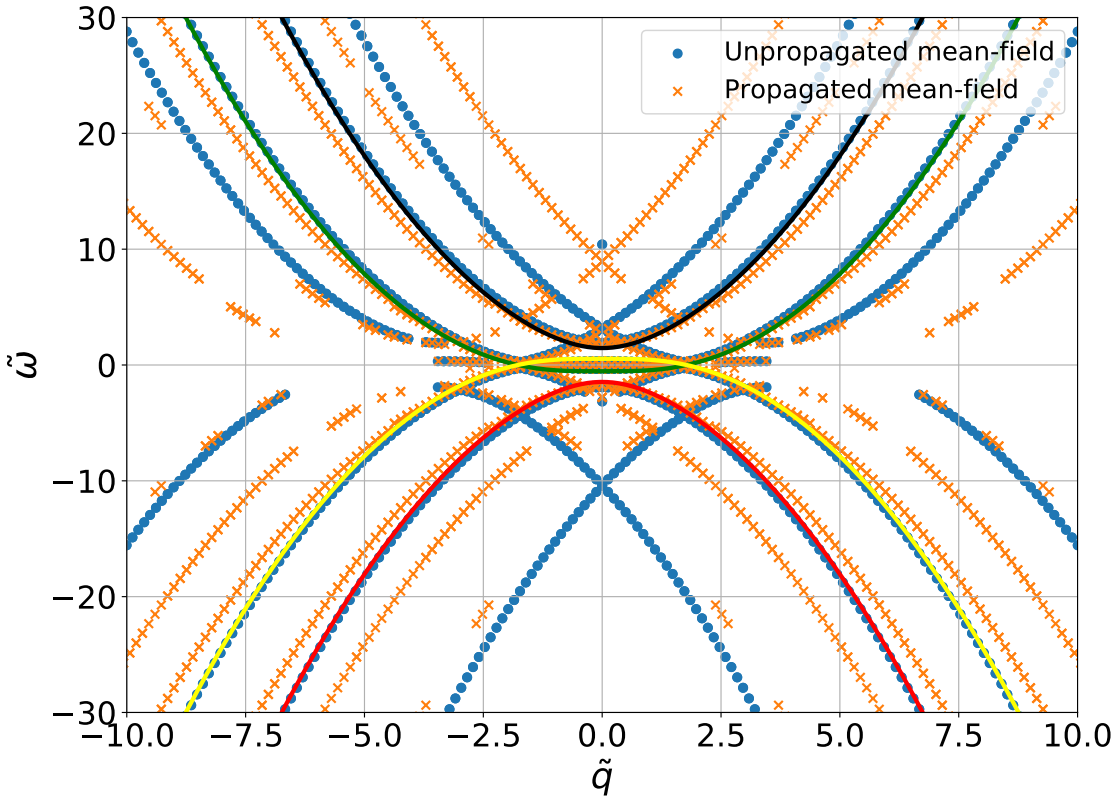


**Figure 5.11:** Numerically calculated excitation spectrum corresponding of the mean-field given by the analytical ansatz before and after propagation. The parameters used here were $\tilde{\Omega} = 1.15$, $\tilde{G}_1 = 0.2$, $\tilde{G}_2 = 0.05$. This is plotted together with the single particle relations relations $\pm\left[-\tilde{\mu} + \tilde{k}_0^2 + \tilde{q}^2 \pm \frac{1}{2}\sqrt{4k_0^2\tilde{q}^2 + \tilde{\Omega}^2}\right]$ for $\Omega = 0.6$ displayed by the filled lines.

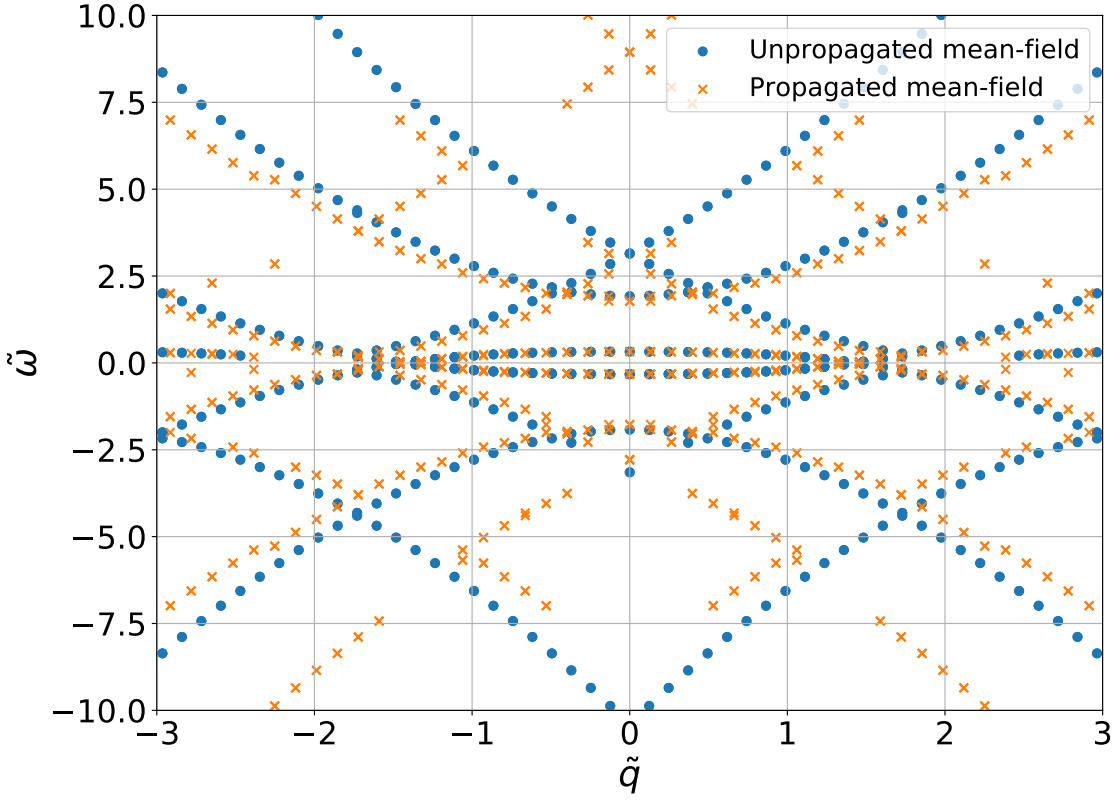


**Figure 5.12:** Numerically calculated excitation spectrum corresponding of the mean-field given by the analytical ansatz before and after propagation. The parameters used here were $\tilde{\Omega} = 1.15$, $\tilde{G}_1 = 0.2$, $\tilde{G}_2 = 0.05$.

# 6
# Conclusion and outlook

By using an imaginary time method in conjunction with a Fourier split-step method, a decrease in the ground state energy was found for a certain set of parameters. This resulted in a shift of the phase transition between phase 1 and 2 as can be seen in Figure 5.8. $\tilde{\Omega}^{(\mathrm{I-II})} = 1.2 \rightarrow \tilde{\Omega}^{(\mathrm{I-II})} = 1.28$ This was the result of finding a higher Fourier component in $\tilde{k}$-space, and could provide helpful data to determine such phase transitions in a lab setting. For the majority of the Raman couplings, the propagated system was close to the variational ansatz, which is to be expected when examining a system with a small coupling, since the ansatz is based on analytical solutions to the single particle Hamiltonian.
Furthermore the Bogoliubov excitation spectrum was examined, and compared to the single particle solutions. These too were deemed to have great similarities to the single particle counterparts, with some deviations introduced from the self interactions of the mean field. The similarities to the single particle solutions are here also to be expected due to the low couplings examined. Furthermore the numerically calculated excitation spectrum of the analytical ansatz was compared to that of the propagated near the transition from the striped phase to the separated phase, where higher Fourier components were found to be most prominent as a result of the propagation. Here it was found that the excitation spectrum of the propagated solutions were close to the unpropagated solutions for small momenta, but deviated from the analytically predicted quadratic solutions found in Section 2.5.
Possible further studies could be to see how the shift in the phase transition for $\Omega$ behaves for bigger $\tilde{L}$, to see if further possible Fourier components could be detected. Moreover, a study of system with greater coupling constants $G_1$ and $G_2$ could potentially be of great interest. This would potentially allow for solutions further from the single particle ansatz and thus make the relaxation of BEC more relevant. Since the self interaction terms of the GPE highly determine the low momentum behaviour of the system. It is thus highly possible to have a highly different low frequency behaviour, and certainly possible that the Landau criteria would be met for greater couplings. Another natural extension of this study considering the Bogoliubov excitations would be to find either a method that calculates each excitation band separately or find a method that separates the excitation bands found in order to make separate analyses on these. Moreover, the since the excitation spectrum of the propagated solutions were assumed to have some deviations from that of the analytical ansatz, an in depth analysis of the superfluidity of the spin-orbit coupled Bose-Einstein condensate near these transition points for relevant couplings.

# Bibliography


[1] Albert Einstein. "Quantentheorie des einatomigen idealen Gases". In: *Sitzung der physikalisch-mathematischen Klasse* (Jan. 1925). URL: https://www.lorentz.leidenuniv.nl/history/Einstein_archive/Einstein_1925_publication/Pages/paper_1925_08.html.

[2] Sébastien Balibar. "The Discovery of Superfluidity". In: *Journal of Low Temperature Physics* 146.5-6 (Jan. 2007), pp. 441–470. DOI: 10.1007/s10909-006-9276-7. URL: https://doi.org/10.1007/s10909-006-9276-7.

[3] E P Gross. "Structure of a Quantized Vortex in Boson System". In: *Nuovo Cimento (Italy) Divided into Nuovo Cimento A and Nuovo Cimento B* Vol: (10) (May 1961). DOI: 10.1007/BF02731494. URL: https://www.osti.gov/biblio/4028087.

[4] Alexander L. Fetter. "Vortices in an Imperfect Bose Gas. IV. Translational Velocity". In: *Phys. Rev.* 151 (1 Nov. 1966), pp. 100–104. DOI: 10.1103/PhysRev.151.100. URL: https://link.aps.org/doi/10.1103/PhysRev.151.100.

[5] Aleksandr F Andreev and I M Lifshitz. "Quantum Theory of Defects in Crystals". In: *Soviet Physics Uspekhi* 13.5 (May 1971), pp. 670–670. DOI: 10.1070/pu1971v013n05abeh004235.

[6] A. J. Leggett. "Can a Solid Be "Superfluid"?" In: *Phys. Rev. Lett.* 25 (22 Nov. 1970), pp. 1543–1546. DOI: 10.1103/PhysRevLett.25.1543. URL: https://link.aps.org/doi/10.1103/PhysRevLett.25.1543.

[7] L. Chomaz et al. "Long-Lived and Transient Supersolid Behaviors in Dipolar Quantum Gases". In: *Phys. Rev. X* 9 (2 Apr. 2019), p. 021012. DOI: 10.1103/PhysRevX.9.021012. URL: https://link.aps.org/doi/10.1103/PhysRevX.9.021012.

[8] Fabian Böttcher et al. "Transient Supersolid Properties in an Array of Dipolar Quantum Droplets". In: *Phys. Rev. X* 9 (1 Mar. 2019), p. 011051. DOI: 10.1103/PhysRevX.9.011051. URL: https://link.aps.org/doi/10.1103/PhysRevX.9.011051.

[9] L. Tanzi et al. "Observation of a Dipolar Quantum Gas with Metastable Supersolid Properties". In: *Phys. Rev. Lett.* 122 (13 Apr. 2019), p. 130405. DOI: 10.1103/PhysRevLett.122.130405. URL: https://link.aps.org/doi/10.1103/PhysRevLett.122.130405.

[10] Yun Li et al. "Superstripes and the Excitation Spectrum of a Spin-Orbit-Coupled Bose-Einstein Condensate". In: *Physical Review Letters* 110.23 (June 2013). ISSN: 1079-7114. DOI: 10.1103/physrevlett.110.235302. URL: http://dx.doi.org/10.1103/PhysRevLett.110.235302.

[11] Spielman et al. “Spin-Orbit Coupled Bose-Einstein Condensates”. In: *Journal of Chemical Education* 471 (Mar. 2011), pp. 83–86. DOI: 10.1038/nature09887.

[12] Yun Li, Lev P. Pitaevskii, and Sandro Stringari. “Quantum Tricriticality and Phase Transitions in Spin-Orbit Coupled Bose-Einstein Condensates”. In: *Phys. Rev. Lett.* 108 (22 May 2012), p. 225301. DOI: 10.1103/PhysRevLett.108.225301. URL: https://link.aps.org/doi/10.1103/PhysRevLett.108.225301.

[13] L.P. Pitaevski and S. Stringari. *Bose-Einstein Condensation and Superfluidity*. International series of monographs on physics. Oxford University Press, 2016. ISBN: 9780198758884. URL: https://books.google.de/books?id=_y4ZswEACAAJ.

[14] I. B. Spielman. “Light induced gauge fields for ultracold neutral atoms”. In: *Annual Review of Cold Atoms and Molecules* (2013), 145–187. DOI: 10.1142/9789814440400_0005.

[15] N Goldman et al. “Light-induced gauge fields for ultracold atoms”. In: *Reports on Progress in Physics* 77.12 (Nov. 2014), p. 126401. DOI: 10.1088/0034-4885/77/12/126401. URL: https://doi.org/10.1088/0034-4885/77/12/126401.

[16] Y.-J. Lin et al. “Bose-Einstein Condensate in a Uniform Light-Induced Vector Potential”. In: *Phys. Rev. Lett.* 102 (13 Mar. 2009), p. 130401. DOI: 10.1103/PhysRevLett.102.130401. URL: https://link.aps.org/doi/10.1103/PhysRevLett.102.130401.

[17] J. A. C. Weideman and B. M. Herbst. “Split-Step Methods for the Solution of the Nonlinear Schrödinger Equation”. In: *SIAM Journal on Numerical Analysis* 23.3 (1986), pp. 485–507. DOI: 10.1137/0723033. eprint: https://doi.org/10.1137/0723033. URL: https://doi.org/10.1137/0723033.

[18] Tobias Ilg et al. *Dynamics of Solitons in the One-Dimensional Nonlinear Schrödinger Equation*. 2016. DOI: 10.48550/ARXIV.1605.06317. URL: https://arxiv.org/abs/1605.06317.

# A

# Appendix

This appendix briefly describe the theory of three systems that were used to test our model. Firstly, the harmonic oscillator and the Pöschl-Teller potential are described, and following the BEC bright soliton solution is explained.

## A.1 Harmonic oscillator

The simple classic 1-dimensional harmonic oscillator has a potential $V(x) = \frac{1}{2}m\omega^2x^2$, such that the system is time-independent and

$$\left(\frac{p^2}{2m} + \frac{1}{2}m\omega^2x^2\right)\Psi = E\Psi \tag{A.1}$$

Gives the energy of the system.
From dimensional analysis it can be shown that the terms on the left hand side of equation A.1 has units of energy, such that dividing both sides by $\hbar\omega$ gives

$$\left(\frac{\hat{p}^2}{2\hbar m} + \frac{m\omega}{2\hbar}\hat{x}^2\right)\Psi = \epsilon\Psi \tag{A.2}$$

such that $\epsilon$ is a dimensionless unit of energy. Similarly, by introducing $p_0 = \sqrt{m\hbar\omega}$ and $x_0 = \sqrt{\hbar/m\omega}$ we can introduce dimensionless parameters as

$$\begin{aligned}\tilde{p} &= \frac{\hat{p}}{\sqrt{2}p_0} \\ \tilde{x} &= \frac{\hat{x}}{\sqrt{2}x_0}\end{aligned} \tag{A.3}$$

This leaves us with a non-dimensional differential equation on the form

$$\left(\tilde{p}^2 + \tilde{x}^2\right)\Psi = \epsilon\Psi \tag{A.4}$$

The energy eigenvalue of this system are on the form

$$\begin{aligned}E_n &= (n + \frac{1}{2})\hbar\omega \\ &\text{or} \\ \epsilon_n &= n + \frac{1}{2},\end{aligned} \tag{A.5}$$

where $n = 0, 1, 2, 3.....$ The ground state wave function $\Psi_0$ is then

$$\Psi_0(\tilde{x}) = \left(\frac{1}{\pi}\right)^{\frac{1}{4}} \exp\left(-\tilde{x}^2\right) \frac{1}{\sqrt{x_0}}. \tag{A.6}$$

## A.2 Pöschl-Teller potential

We shall here present a subset of the Pöschl-Teller potential which we shall here define as the potential having the ground state of

$$\psi_0 = \sqrt{\frac{N}{L}} \mathrm{sech}^l(x/x_0) \tag{A.7}$$

in the presence of the standard one dimensional Schrödinger equation. Here $x_0$ and $L$ are simply some arbitrary length scale and $N$ is a normalization constant. Thus it is defined such that $V(x)$ fulfills

$$-\frac{\hbar^2}{2m}\frac{d^2}{dx^2}\psi_0(x) + [V(x) - E_0]\,\psi_1(x). \tag{A.8}$$

Using the fact that

$$\frac{d^2}{dx^2}\mathrm{sech}(x) = [1 - 2\mathrm{sech}(x)]\,\mathrm{sech}(x), \tag{A.9}$$

one obtains

$$V(x) - E_0 = \frac{\hbar^2 l}{2m}\sqrt{\frac{N}{L}}(l - (l+1)\,\mathrm{sech}^2(x/x0)) \tag{A.10}$$

and hence

$$V(x) = -C\frac{l(l+1)}{2}\mathrm{sech}^2(x/x_0) \tag{A.11}$$

where $C = \hbar^2/m \cdot \sqrt{N/L}$. For $l = 1$ a simple analytic solutions for the ground state can be identified by setting the wave function to

$$\psi_0(x) = \sqrt{\frac{N}{L}}\mathrm{sech}(x/x_0) \tag{A.12}$$

where for $x_0 = 1$ one has that $\sqrt{N/L} = 1/\pi$ and $E = -0.5$.

## A.3 Bright soliton

For a few specific GPEs, there exists analytical solutions, for example for the so called bright soliton solutions for an attractive potential with a negative coupling constant $g$ [18]. Here we shall present the 1D-case for $V(x) = 0$, and redefine $g$ to be positive so that the Hamiltonian reads

$$H = -\frac{\hbar^2}{2m}\frac{d^2}{dx^2} - g|\psi|^2 \tag{A.13}$$

which can be shown to have the ground solution of

$$\psi(x,t) = A \text{ sech}\left[\left(2m|\mu|/\hbar^2\right)^{1/2} x\right] \tag{A.14}$$

where $A$ is some normalization constant of units $[\text{L}]^{-1/2}$ and $\mu^2/2 = g$ [18]. To see that this wavefunction is an actual solution to the eigenvalue problem with a Hamiltonian given by Equation (A.13), we shall simply substitute it into $H\psi$, and using the fact that

$$\frac{d^2}{dx^2}\frac{1}{\cosh(x)} = \tanh^2(x)\text{sech}(x) - \text{sech}^3(x) \tag{A.15}$$

one finds that

$$\begin{aligned} H\psi &= -A\sqrt{2\mu}\text{sech}(\alpha x)\left(\frac{\hbar^2}{2m}\alpha^2\left(\tanh^2(\alpha x)\text{sech}^3(\alpha x)) - \text{sech}^3(\alpha x)\right) + 2\mu \text{ sech}(\alpha x)\right) \\ &= -A\sqrt{2\mu}\text{ sech}(\alpha x)\ \mu\left(\frac{\sinh^2(\alpha x) + \cosh^2(\alpha x) - \sinh^2(\alpha x)}{\cosh^2(\alpha x)}\right) = -\mu\psi \end{aligned} \tag{A.16}$$

where for simplicity we have defined $\alpha = (2m|\mu|/\hbar^2)^{1/2}$.

**DEPARTMENT OF SOME SUBJECT OR TECHNOLOGY**
**CHALMERS UNIVERSITY OF TECHNOLOGY**
Gothenburg, Sweden
www.chalmers.se


CHALMERS
UNIVERSITY OF TECHNOLOGY